Journal of Structural Dynamics, 3, (pp. 30-57) 2025
A novel analysis method for calculating nonlinear Frequency Response Functions

Journal of Structural Dynamics

A novel analysis method for calculating nonlinear Frequency Response Functions

D. Di Maio*[1]

[1] *University of Twente, Faculty of Engineering Technology, MS³ department De Horst 2, 7522 LW, Enschede, the Netherlands*

Abstract

This research presents a novel analysis method for calculating nonlinear Frequency Response Functions from a *nonlinear frequency response surface* (*NFRS)*. The research aims to provide engineers with a user-friendly technique to evaluate the nonlinear frequency responses when the modal parameters as a function of the vibration amplitude are available. The Frequency Response Functions (*FRFs*) are the most widely used functions to characterise the dynamic behaviour of structures. The experimental modal analysis stands on four pillars 1) measurement, 2) identification, 3) regeneration, and 4) comparison, and these four steps must be ensured under linear and nonlinear vibrations. However, the nonlinear vibrations are challenging for identifying, regenerating, and comparing nonlinear *FRFs*.

This research postulates that a nonlinear *FRF* solves a geometrical intersection between the *nonlinear frequency response surface* and any constant amplitude force surface. The paper demonstrates the hypothesis with ONE- and TWO-DoF systems with a cubic stiffness nonlinearity by showing how to generate a *nonlinear frequency response surface* when the force-displacement relationship is calculated. The verification of the proposed formulation is yielded by comparing nonlinear *FRFs* generated by the new analysis method (*NM*) to the ones generated by the Harmonic Balance Method and numerical integration. Furthermore, the paper presents a new identification method, based on the Dobson formulation, for extracting amplitude-dependent modal parameters. These parameters generate an *NFRS*, from which synthesised nonlinear *FRFs* are evaluated and compared to the experimental ones. The most important innovation of this research is that the four steps listed earlier can quickly be implemented with the proposed technique.

Keywords: Frequency Response Surface, modal analysis, nonlinear *FRF*

Received on May 17, 2024, *Accepted on December 18, 2024*, *Published on January 21, 2025*

1 Introduction

Modal testing and analysis are well-established practices for measuring and analysing frequency response functions. The modal parameters identified from the analysis can be used to generate a simple mathematical response model or validate and update a structural model generated by finite element methods. There are four essential steps in the modal analysis practice. The first one is the measurement of frequency response frequencies, *FRFs*, which are the ratio between response and stimulus, measured under steady-state, random or transient vibrations. The vibrations are acquired and processed by linear operators, such as the Fast Fourier Transform (*FFT*), to calculate frequency response spectra. The second step is the modal analysis, which identifies the modal parameters from the *FRFs*. The process can be either via time- or frequency-domain methods. The third step is to generate or synthesise *FRFs* using linear frequency response models with the modal parameters identified in the second step. The final fourth step is the comparison of the measured and synthesised *FRFs*, a process that ensures the reliability of the modal parameters. Nowadays, modal analysis toolsets are implemented in several commercial and open-source software suites and used in several engineering applications. The four steps, 1) measurement, 2) identification, 3) regeneration and 4) comparison, ensure that the analysis process delivers robust and reliable modal parameters. Ewins [1], Maia [2], Avitable [3], to name a few, worked extensively on modal analysis, and they cast this modus operandi on solid foundations for the future generation of practitioners to use it reliably.

* d.dimaio@utwente.nl

Any mechanical system is intrinsically nonlinear by nature, and therefore, those four steps described earlier break as soon as nonlinear vibrations are excited and measured. Under such nonlinear conditions, the *FRFs* will become more and more distorted. Such distortions can become visible around the resonances, which tend to skew towards higher or lower frequencies. There are also situations where the resonance distortion is not visible. Therefore, any modal test practitioner must often conduct linearity checks before running any test. Tomlinson and Worden wrote a textbook describing nonlinear structural dynamics [4], in which several types of nonlinearities are modelled in the frequency and time domain, and experimental techniques for characterising nonlinearities are also presented. Although nonlinear dynamics is a science that covers many applications, from engineering to physics and mathematics, this manuscript narrows its focus to the steady state nonlinear vibrations, which are only analysed using *FRFs*.

Noël and Kerschen [5] wrote a comprehensive manuscript reviewing the testing and identification methods developed from 2006 to 2016. The author's interest in that review is on the methods focussed on *FRF* linearisation and the CONCERTO techniques, both of which evaluate amplitude-dependent modal properties from *FRFs* measurements. The review highlights the pros and cons of those techniques, which will be discussed further in section 3.1 of this paper. Moreover, consistent research work on the test and analysis of nonlinear *FRFs* was carried out by Özgüven et al. [6-9], which is the primary source of inspiration for the proposed analysis method. Özgüven [9] describes a response surface in his manuscripts, generated by the frequency, harmonic displacement and force. That surface is called the Harmonic Force Surface (HFS). The authors report that: "*In Response Controlled Test, this problem is solved by keeping the displacement amplitude constant, which results in smooth response spectrum incorporating points on the unstable branch as well*." The authors also report that equation (24) in [9] is solved iteratively to synthesise the nonlinear frequency response. Despite the high value of that research, this manuscript takes a different direction by using a simple open-loop control method for measuring and analysing one nonlinear *FRF*. Since 2019, Zhang and Zang [10-12] proposed an interesting testing technique for characterising nonlinear vibrations. Their technique can also extract amplitude-dependent modal parameters from several FRFs measured using an open-loop control technique. A further in-depth description of their technique is given in section 3.1. Their research also inspired this paper, but it takes a step further by demonstrating that a single nonlinear *FRF* is sufficient for retrieving amplitude-dependent parameters even when one part of the *FRF* branch is missing because of the unstable vibration response. The yielding of the nonlinear modal parameters is also used to generate a *nonlinear frequency response surface*.

This manuscript postulates that:
A nonlinear frequency response surface, generated by a waterfall of linear FRFs, is the solution space of nonlinear FRFs, which can be evaluated by any force plane cutting across the response surface.

The hypothesis must address the following scientific objectives:

(i) The primary scientific objective is to develop a new mathematical formulation to (i) analyse a *nonlinear frequency response surface* and (ii) calculate nonlinear frequency response functions.

(ii) The secondary scientific objective is to develop a new modal analysis tool to calculate amplitude-dependent modal parameters using one *FRF* rather than several ones.

This manuscript will present three research sections. The first section will focus on one and two degrees of freedom systems to model and simulate a *nonlinear frequency response surface*. At this stage, the nonlinearity is achieved using a nonlinear force-displacement relationship. The nonlinear *FRF*s evaluated by the proposed method are compared to nonlinear *FRFs* calculated by numerical integration and the Harmonic Balance Method. The second section will present a novel modal analysis method based on the Dobson formulation [13], which allows for calculating amplitude-dependent modal parameters from one nonlinear *FRF*. These modal parameters will be used to generate the *NFRS*. Finally, the third section will present three case studies to validate the new formulation proposed: one experimental case based on a lap joint and two experimental cases based on a composite blade. In this section, the regeneration and comparison of the *FRFs* are yielded to prove the validity of the hypothesis. A blind analysis, the fourth case, is also provided to show that the entire process is achieved on test data generated from an unknown aerospace component.
It is important to stress that the proposed formulation and application of the method are currently developed on the following limitations.

(i) Experimental and synthesised measurements are yielded using stepped sine tests under steady state conditions.

(ii) The *FRFs*, calculated from the measurements, are the ratio between the response and stimulus at the fundamental excitation frequency, and therefore, higher-order harmonics are neglected.

(iii) The resonances are considered well-isolated, meaning that modal contribution from neighbouring modes can be neglected.

(iv) The manuscript focuses on smooth nonlinearities.

2 Response function model for nonlinear steady state vibrations

The primary scientific objective of this section is to demonstrate the hypothesis postulated in the introduction. The investigation starts by revisiting the relationship between force and displacement, which contains an element to understand how linear *FRFs* can generate a *nonlinear frequency response surface*. This section will only treat a grounded nonlinear stiffness, leaving the nonlinear damping out of the scope of this demonstration. The nonlinear *FRF* yielded by the proposed new analysis method (*NM*) will be compared to those calculated using the Harmonic Balance Method and numerical integration method. The section will focus on the ONE- and TWO-Degrees of Freedom systems to prove that an *NFRS* can be simulated with a cascade of linear *FRFs*, and any nonlinear *FRF* is the geometrical intersection between the response and stimulus surface.

2.1 Force-displacement relationship for linear system

An idealised spring, subjected to a static force, will extend or compress about a displacement, (X). It is custom to write the force-displacement relationship as in equation (1), where k, is the stiffness coefficient. An alternative form can be used, in which equation (1) describes the compliance of the spring as expressed by equation (2).

$$F(X) = kX \tag{1}$$

$$\frac{X}{F(X)} = \frac{1}{k} = \alpha(X) \tag{2}$$

One can plot the relationship of the compliance as a function of displacement, and this plot bears a critical significance when the static compliance (or receptance) is extended over the frequency domain. First, we shall assume that a spring and a mass, m, are subjected to a harmonic force, which will lead to a harmonic response as expressed by equation (3), where ω is the excitation frequency. The transfer function of the spring and the mass are expressed by equation (4). The transfer function of the spring itself does not depend on the excitation frequency. The transfer function of the mass depends on the inverse of the squared of the excitation frequency. When the two transfer functions are plotted in the Bode diagram (log-log scale), these will be two straight lines forming the skeleton of the *FRF* [14]. The intercept of the two straight lines occurs at the undamped natural frequency of the sprung-mass system. By adding damping, the skeleton can be dressed using the equation (5), where c, is the viscous damping.

$$x(t) = Xe^{i\omega t}\ f(X,t) = F(X)e^{i\omega t} \tag{3}$$

$$\frac{X}{F(X)} = \frac{1}{k} \quad \text{(a)} \qquad \frac{X}{F(X)} = -\frac{1}{m\omega^2} \quad \text{(b)} \tag{4}$$

$$\frac{X}{F(X)}(\omega) = \frac{1}{k - m\omega^2 + i\omega c} \tag{5}$$

In conclusion, by using equation (5), one can simulate a linear *FRF* from any point of the static compliance function. The waterfall of linear *FRFs* generates a *linear frequency response* surface, and any force plane used for cutting across that surface will return a linear *FRF*, as expected. **Fig. 1** shows a 3D plot of the Bode diagram, where the static receptance is constant and the start of linear *FRFs*, whereas the dashed red lines are possible static forces which will extend over the frequency axis at constant amplitude (or slope).

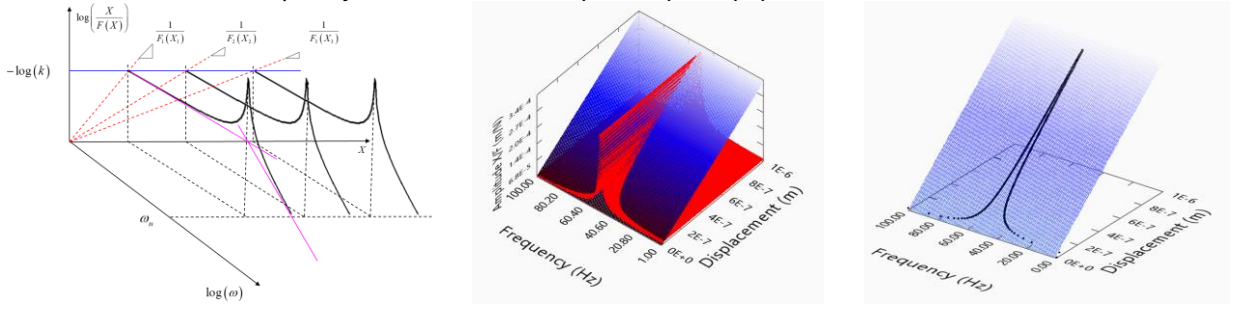

(a) (b) (c)

Fig. 1: (a) Schematic Linear Frequency Response Surface (*LFRS*), (b) simulated of the *LFRS* and (c) projection of the linear *FRF* on the force plane

2.2 Force-displacement relationship for nonlinear system

Understanding that the linear frequency response surface is the solution space of any possible linear FRF was straightforward. This section repeats the process using the linear equation of motion, expressed by the transfer function in equation (5). It is rewritten using a cubic stiffness nonlinearity in equation (6). The relationship between force and displacement is nonlinear, for which k_{LIN} is the linear stiffness coefficient and k_{NL} is the nonlinear one. Assuming both harmonic force and response, as given in equation (3), one calculates the static transfer function for $\omega = 0$. Equation (7) shows the static receptance for linear (a) and nonlinear responses (b). These two static transfer functions are plotted in **Fig. 2**.

The next step is to repeat the procedure as described earlier. A cascade of linear *FRFs* will be generated using equation (9) starting from the nonlinear static transfer function $\alpha(X)$.

$$m\ddot{x} + c\dot{x} + k_{LIN}x + k_{NL}x^3 = f(x,t) \tag{6}$$

$$\frac{X}{F(X)}(\omega = 0, X) = \alpha(X) = \frac{1}{k_{LIN}} \quad \text{(a)}$$
$$\frac{X}{F(X)}(\omega = 0, X) = \alpha(X) = \frac{1}{k_{LIN} + k_{NL}X^2} \quad \text{(b)} \tag{7}$$

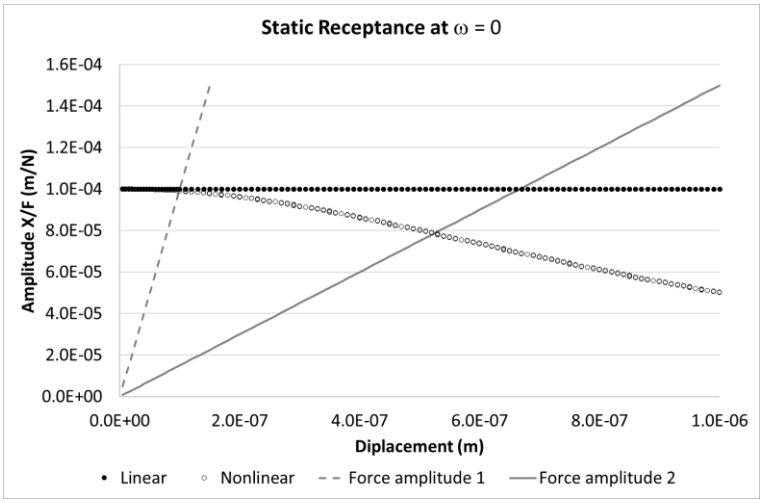

Fig. 2: Linear and nonlinear static receptance curves

As indicated earlier, every point of the nonlinear static receptance can be the starting point of a linear *FRF,* as shown in **Fig. 2**. The effective stiffness, k_E, can be calculated by the equation (8), noting that one effective stiffness exists for one force, $F_i(X)$, where, i, indexes the force amplitude (see **Fig. 2**). Equation (9) is used for generating the

$$k_E(X) = \frac{X}{F_i(X)}$$
$$i = 1 \ldots n \tag{8}$$

nonlinear frequency response surface (*NFRS*) for the single degree of freedom system.

$$\alpha(\omega, X) = \frac{1}{k_E(X) - m\omega^2 + i\omega c} \tag{9}$$

Fig. 3 shows an *NFRS* generated between 0 and 100 Hz in a displacement range between 0 and 1*10^{-6} m in the colour spectrum. The surface is built with many linear *FRFs* which follow the pattern set by the nonlinear static receptance. **Fig. 2** shows two forces of different amplitudes, and equation (10) evaluates the receptance amplitudes for a given force amplitude, which will extend over the frequency range, as expressed by equation (11). This force surface cuts across the *NFRS*, as shown in **Fig. 4**. A nonlinear *FRF* curve is visible on that force surface, as shown

$$|\bar{\alpha}(X)| = \frac{X}{F_i(X)} \tag{10}$$

in **Fig. 5**.

$$F_i(\omega, X) = \frac{X}{|\bar{\alpha}(\omega,X)|} \tag{11}$$

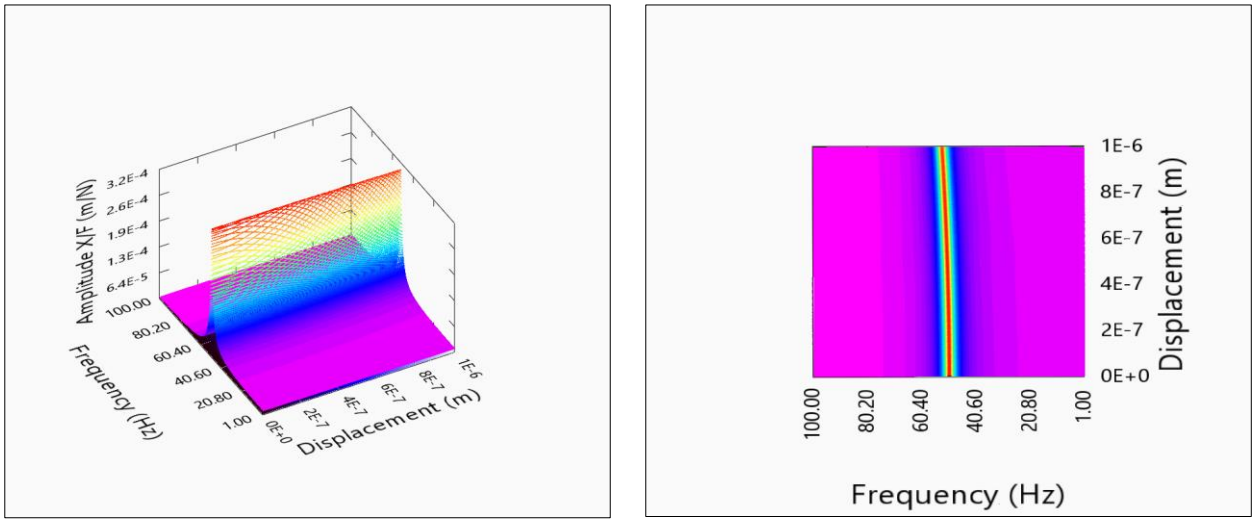

a) Perspective. b) Top-view.

Fig. 3: *Nonlinear frequency response* surface

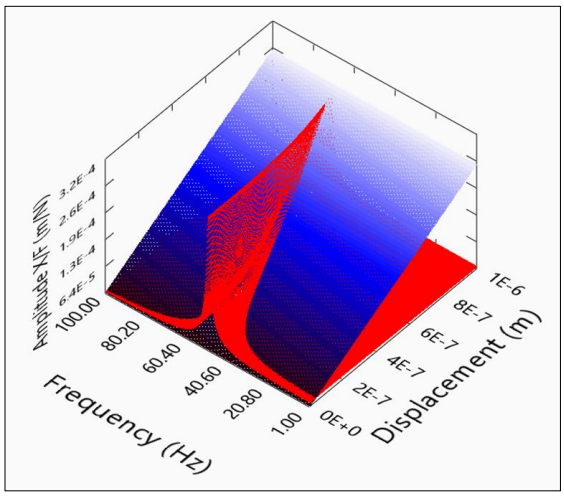

Fig. 4: *Nonlinear frequency response* surface (red) and constant force plane (blue)

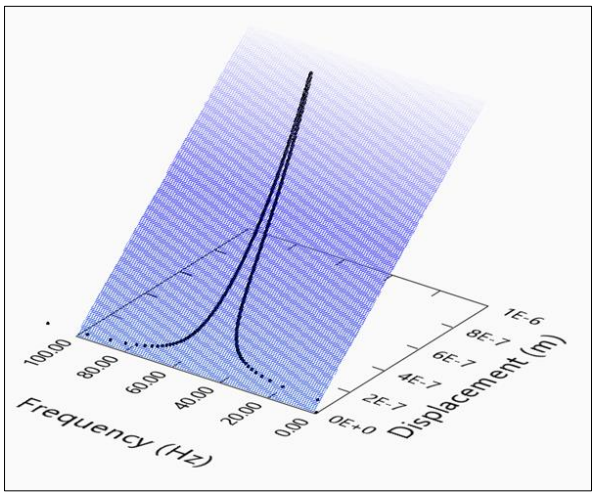

Fig. 5: Nonlinear *FRF* overlaid on the force surface

The final step is to extract the nonlinear *FRF*, a geometrical intersection between two surfaces, the response and the stimulus. This step is achieved using equations (12) and (13). At this stage, one should note that there is an excitation frequency used for generating the surfaces and an unknown variable called frequency, ω_{NL}, which is the frequency evaluated by the intersection of these two surfaces. The receptance amplitudes, $|\bar{\alpha}(\omega, X)|$, are known at every displacement amplitude (see the plot in **Fig. 2**), and the effective stiffness is calculated from equation (7), whereas the mass, m , and the damping, c, are taken from the **Table 1**. Reworking the equation (12) as function of the unknow frequency, ω_{NL}, one can solve an equation of the fourth order, equation (13), which will give four roots for the selected receptance value. Once the nonlinear frequency, ω_{NL}, is calculated for every linear *FRF* at a given receptance amplitude (eq.(11)), the real and imaginary parts of the nonlinear receptance can be calculated using equations (14) and (15). The undamped natural frequency, ω_r, is calculated by the ratio between the effective stiffness, $k_E(X)$, at displacement (X), and the mass m. One will be able to generate the full nonlinear *FRF* for any desired force amplitude, as shown in **Fig. 6**.

$$|\bar{\alpha}(\omega, X)| = \left|\frac{1}{k_E(X) - m\omega_{NL}^2 + i\omega_{NL}c}\right| \tag{12}$$

$$\omega_{NL}^4 + \left(2mk_E(X) - \frac{cmk_E(X)}{\sqrt{mk_E(X)}}\right)\omega_{NL}^2 + \frac{k_E^2(X)}{m^2} - \frac{1}{|\bar{\alpha}(\omega,X)|} = 0 \tag{13}$$

$$RE_{1,2} = \omega_r^2 - \omega_{NL1,2}^2 \tag{14}$$

$$IM_{1,2} = 2\zeta * \omega_r * \omega_{NL1,2} \tag{15}$$

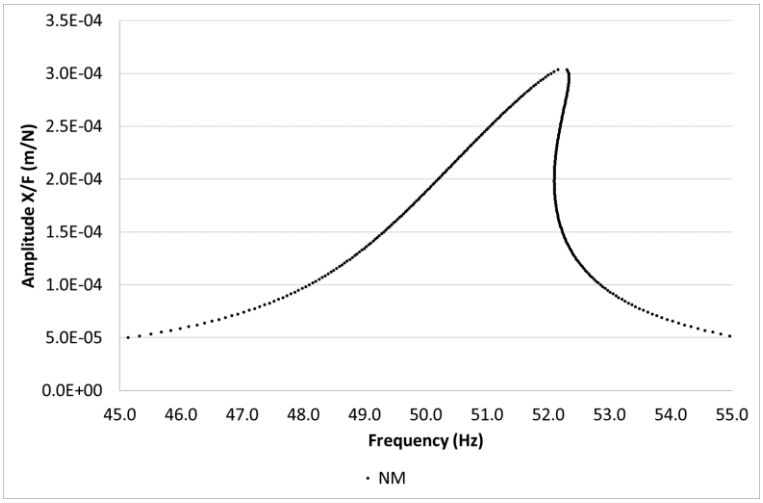

Fig. 6: Nonlinear *FRF* calculated from the *nonlinear frequency response* surface

The verification of the nonlinear *FRF*, thus calculated, is carried out by numerical integration (ODE) and the Harmonic Balance Method (HBM). A single DOF equation of motion (16) generates nonlinear *FRFs*. The system parameters implemented in the equation (16) are listed in the Table 1. The simulation of the nonlinear *FRF* was run between 40 and 60 Hz with a frequency step of 0.1 Hz, and every step was simulated for 2 seconds at 10,000 samples/sec. The HBM is performed using the first fundamental harmonic, as many textbooks show. Instead of the modulus and phase, the real and imaginary parts of the *FRF* are calculated to plot the Nyquist circles. **Fig. 7** shows Nyquist curves for the three calculated *FRFs*, which overlay on each other.

$$\ddot{x} + 2\zeta\omega_r\dot{x} + \omega_r^2 x + k_{NL}x^3 = p = \frac{f(t)}{m} = P\,cos(\Omega t + \phi) \tag{16}$$

Table 1: SDOF system parameters

Mass	Damping	Linear stiffness	Nonlinear stiffness
m = 0.1 kg	c = 1 m/s N^{-1}	k_{LIN} = 10^4 N/m	k_{NL} = 1^{15} N/m^3

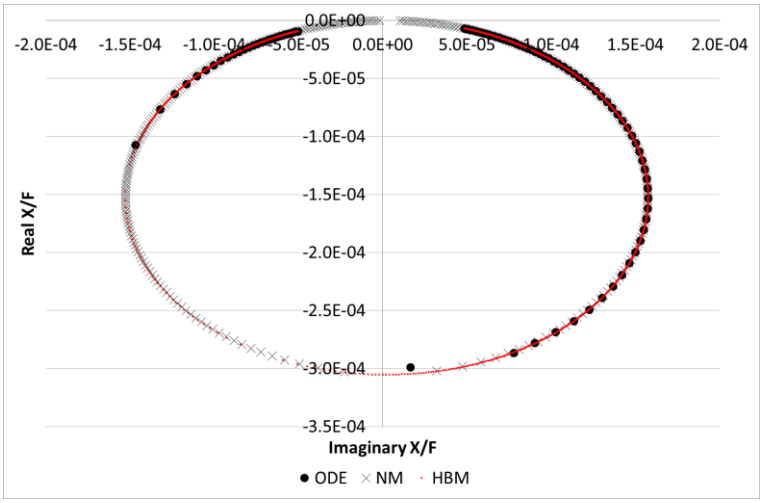

Fig. 7: Comparison of the Nyquist circles simulated by numerical integration (ODE), the new method (NM) and the harmonic balance method (HBM)

This section proves that a nonlinear frequency response surface can be simulated using a linear frequency response model, and the section ends by comparing three nonlinear *FRFs*. The main objective was to evaluate a nonlinear

FRF resulting from a geometrical intersection between two surfaces, the stimulus and response. This formulation supports the new analysis method when nonlinear modal parameters are extracted from nonlinear *FRFs*. The following subsection will extend the analysis method to a TWO-DoF vibration response to verify that the two surfaces can extract a nonlinear *FRF* for an MDoF system.

2.3 The theoretical nonlinear transfer function for a TWO-DoF system

This subsection investigates the proposed analysis method using a TWO-DoF system. One of the hypotheses of this paper is to apply the nonlinear regeneration technique to experimental *FRFs*, which are measured from multiple degrees of freedom systems. Therefore, the extension to MDoF vibration response is necessary for evaluating if the intersection between stimulus and response surfaces generates a nonlinear *FRF*. The previous subsection presented equation (13) for solving the nonlinear *FRF*, while this subsection will provide a more convenient numerical alternative.

As said, this subsection extends the same theoretical formulation to a TWO-DoF system with a grounded stiffness nonlinearity, as shown in **Fig. 8**. This simple system could be imagined as a double cantilever beam, where an end of which has a smaller cross-section area than the other end of the beam, as seen in [15]. The assumptions used in generating this MDoF system will simplify the mathematical formulation, but the model cannot be generalised. The system is made of two masses, m, and three equal linear springs, k_{LIN}, one of the two grounded springs will exhibit nonlinear behaviour, as shown in **Fig. 8**. This simplification makes the stiffness matrix depend on one linear and nonlinear stiffness moduli, which, in reality, might not be the case. Another simplification is grounded nonlinearity, which is a convenient choice to make the receptance as a function of one degree of freedom because the nonlinearity does not couple the two degrees of freedom. Even this simplification does not represent the reality of the response vibrations of structures. Both simplifications show that a constant force plane can extract nonlinear *FRFs* from an MDoF system with modes well separated in frequency. The proof of concept is crucial for section 4, where the experimental validation of the identification and regeneration techniques are applied to real experimental MDoF cases.

The equations of motion are written for the undamped system and presented in equation (17). Table 2 reports the system's and simulations' parameters for the steady state analysis using numerical integration, which will simulate a nonlinear *FRF*.

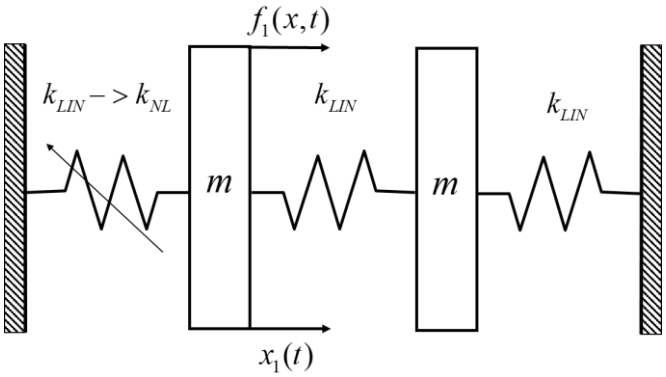

Fig. 8: TWO-DoF system with grounded nonlinearity

Table 2: System parameters and measurement parameters for the steady state simulations

Mass (kg)	Stiffness (N/m)	Damping Ns/m	Nonlinear stiffness (N/m^3)	Excitation force (N)	Frequency step (Hz)	Sample rate Sample/sec	Time generation (sec)	Steady-state part (sec)
0.1	15,000	1	10^{14}	0.00124	0.05	10,000	2	0.3

Under steady state conditions, one can assume a harmonic excitation and response, as expressed in equation (3), and then solve for the transfer function at the first degree of freedom. $x_1(t)$, as expressed in equation (18). That equation will be evaluated at a null frequency on the static receptance plot to learn how the nonlinear stiffness relationship is related between the input and output at the first DoF of the system.

$$\begin{cases} m\ddot{x}_1 + k_{LIN}x_1 + k_{NL}x_1^3 + k_{LIN}(x_1 - x_2) = f_1(x,t) \\ m\ddot{x}_2 - k_{LIN}(x_1 - x_2) + k_{LIN}x_2 = 0 \end{cases} \tag{17}$$

The undamped transfer function is written as follows.

$$\frac{X_1}{F_{1,i}}(\omega, X) = \frac{2k - m\omega^2}{-m\omega^2(2k - m\omega^2) + k(2k - m\omega^2) + k_{NL}(2k - m\omega^2)X_1^2 e^{2\omega t} + k(2k - m\omega^2) - k^2} \tag{18}$$

The static nonlinear receptance is expressed by equation (19), and it allows calculating the effective nonlinear stiffness as a function of the displacement of the degree of freedom, X_1, and a force amplitude, $F_{1,i}$, at the same degree of freedom. When the nonlinearity is null, the static transfer function returns the same value for all displacements, as expected for linear vibrations.

$$\alpha_{1,1}(X) = \frac{X_1}{F_{1,i}} = \frac{1}{k_E(X)} = \frac{2k_{LIN}}{2k_{LIN}k_{NL}X_1^2 + 3k_{LIN}^2} \tag{19}$$

A direct method is used for evaluating the entire receptance matrix, equation (20), valid for the system shown in **Fig. 8**, and for which the effective stiffness is calculated from equation (19). The *NFRS* is generated using the receptance excited and measured at the first degree of freedom as a function of a generic displacement. The stiffness term will obey the relationship expressed in equation (19). The same equation is used for constructing the force plane, which is a function of ω and X, as in equation (11).

$$[\alpha(\omega, X)] = ([K(X)] - \omega^2[M] + i\omega[C])^{-1}$$
$$[K(X)] = \begin{bmatrix} 2k_E & -k_E \\ -k_E & 2k_E \end{bmatrix} \tag{20}$$

Fig. 9 shows the *nonlinear frequency response surface* generated by the equation (20). **Fig. 10** shows a top view of that figure where the variation of the resonance frequency of the first and second modes vary as a function of the displacement. The process of evaluating the nonlinear *FRF* is the one explained earlier. Fig. 11 shows the surface (red) cut across by an arbitrary force surface (blue). Extracting the nonlinear *FRF* from the surface would require solving the equation (20) where the nonlinear frequency, ω_{NL}, is the unknown parameter and the amplitude of the static transfer function is known at every displacement amplitude. The analytical solution for the nonlinear excitation frequency can be very cumbersome, so a much simpler solution technique is offered.

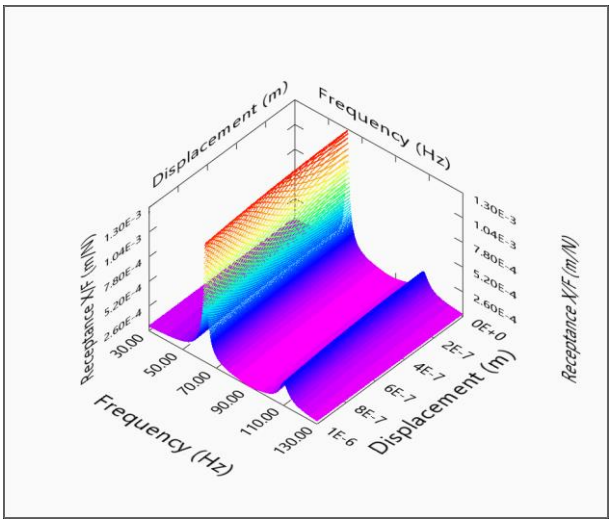

Fig. 9: *Nonlinear frequency response* surface generated by equation (20)

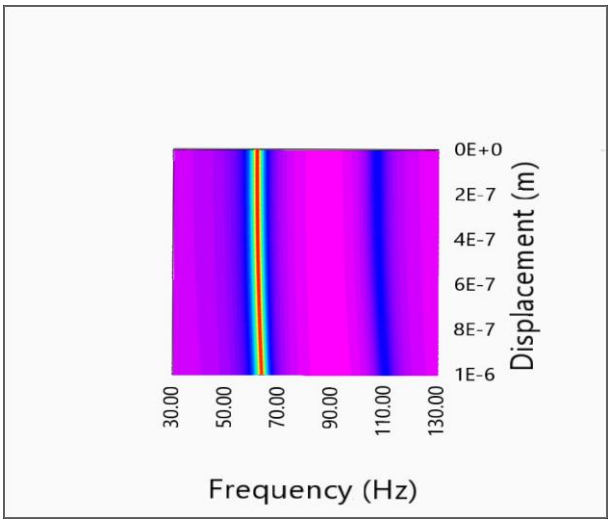

Fig. 10: Top-view of the *Nonlinear frequency response* surface

The product shown in equation (21) equals unity for frequencies evaluated at the same given transfer function modulus, $|\bar{\alpha}_{1,1}(\omega, X)|$, calculated using (19); otherwise, it is different. Note that the overscored receptance is determined by the amplitude of the force plane selected (the blue plane in **Fig. 11**). A numerical solution is used for calculating the new nonlinear frequency, ω_{NL}, for which a search condition is implemented. The finer the frequency steps forming the linear *FRF* of the *nonlinear frequency response* surface, the smaller the error for the search condition that can be set.

$$|\bar{\alpha}_{1,1}(\omega, X)|([K(X)] - \omega_{NL}^2[M] + i\omega_{NL}[C])| = 1 \tag{21}$$

The first verification is done by setting the nonlinear coefficient to null, extracting a linear *FRF* compared to one generated by numerical integration. The numerical integration was somewhat redundant, but consistency was maintained with the simulation when the nonlinearity was activated again. **Fig. 12** shows the comparison and the perfect overlay between the two *FRFs*.

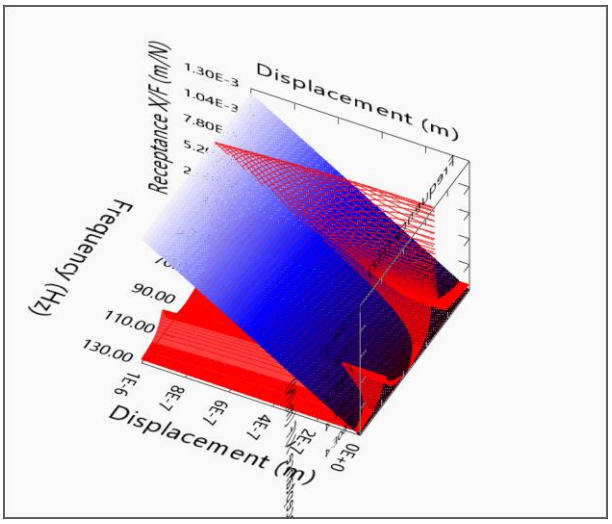

Fig. 11: *Nonlinear frequency response* surface (red) and a constant force plane (blue) for the extraction of the nonlinear *FRF*

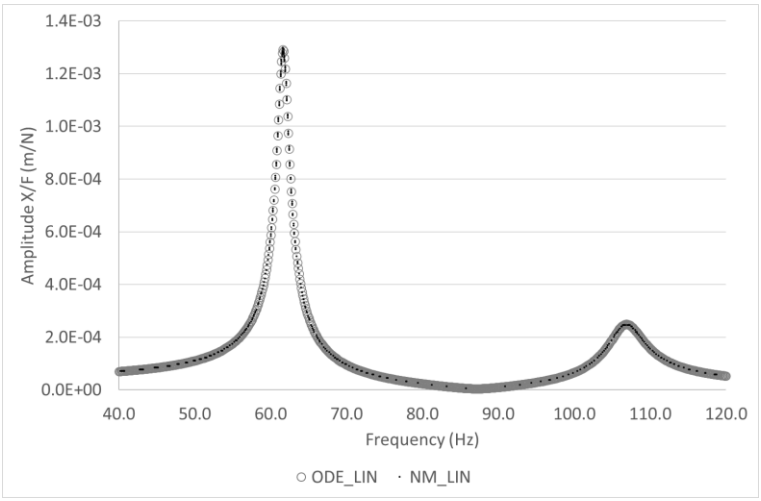

Fig. 12: Comparison between linear *FRF* using numerical integration and NM.

The second simulation is yielded by activating the nonlinearity, setting the nonlinear stiffness coefficient of the cubic term to the value listed in Table 2. The *FRF* extracted from the surface is overlaid by the one generated by the numerical integration, as shown in **Fig. 13**. Both the amplitude and phase of the *FRFs* overlay well, for which the first mode shows a more distinct nonlinearity than a much milder one of the second mode. The simulation of the nonlinear *FRF* yielded by numerical integration presents the typical response jump for the unstable branch of the *FRF*. The nonlinear *FRF* evaluated by the surface will also show the unstable branch, and the missing points of that branch are caused by the frequency steps used by equation (20); the finer the frequency steps, the smoother the regeneration of the nonlinear *FRF*.

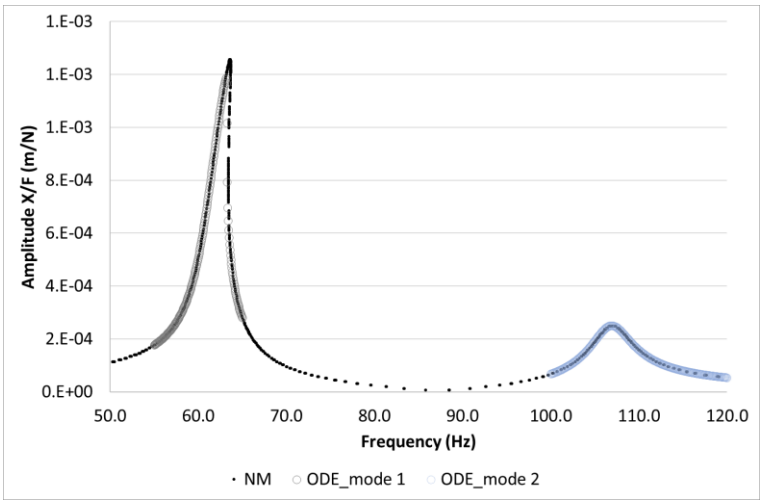

(a) nonlinear *FRF* modulus

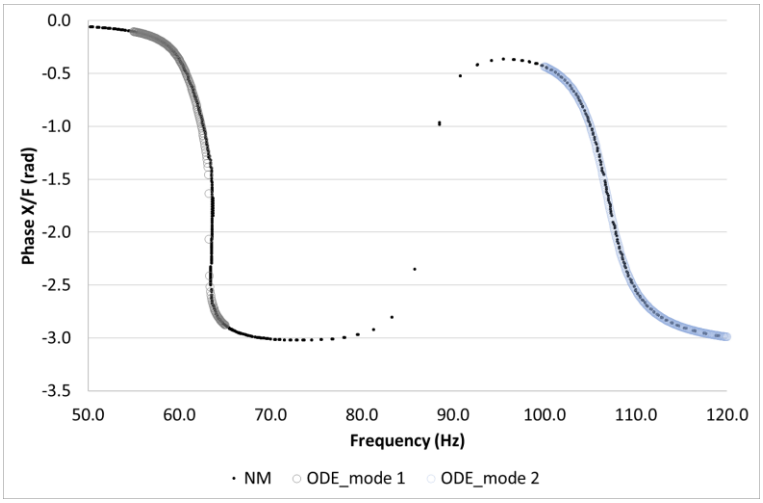

(b) nonlinear *FRF* phase

Fig. 13: Nonlinear *FRF* generated by the new analysis method and numerical integration

2.4 Final remarks

This section showed that a *nonlinear frequency response surface* can be generated using ONE- and TWO-DoF response models with a grounded nonlinearity. In these two examples, the static equivalent stiffness is used to calculate linear *FRFs,* which will build a nonlinear surface. In section 4, the equivalent stiffness will be a function of the natural frequency curve (amplitude-dependent). The *NFRS* will be built using that frequency curve and the other modal parameters such as damping and modal constant. This theoretical section verified the first hypothesis, which is recalled as follows:

(i) *The primary scientific objective is to develop a new mathematical formulation to (i) analyse a nonlinear frequency response surface and (ii) calculate nonlinear frequency response functions*.

Using the TWO-DoF model with grounded nonlinearity is simplistic but proves the new analysis method. The matter would have been more complex if the nonlinear is between two DoFs, whereby the two degrees of freedom will stay coupled. An alternative might be found using Finite Element modelling by Singh et al.[16], the authors use mode shapes to perform virtual fully reverse mechanical loading to extract the equivalent stiffnesses. Magi et al. [17] and Di Maio et al. [18] applied a similar technique where the deflection shape method was used for calculating the energy release rate (ERR) of fatigue damage growth. The second objective of this paper is to prove that such a surface, generated by the experimentally measured amplitude-dependent modal parameters, is the solution space for nonlinear *FRFs*. This further step will require the development of a novel identification method for performing modal analysis.

3 Modal analysis of nonlinear response functions

An extensive review was carried out by Noël and Kerschen [5], and the reader is invited to consult that reference alongside the brief literature presented hereafter. This section is focused on identification methods of nonlinear modal parameters that can be extracted by *FRF* analysis using the single input, single output (SISO) sine testing method. Such a testing method fits the Dobson formulation for linear and nonlinear system identification, described in the following section.

3.1 Background literature

Measuring the frequency response functions is the most used experimental technique for characterising smooth nonlinearities. Although time-consuming because it requires steady state conditions, the stepped-sine test is convenient because it deals with sine IN - sine OUT (+ noise + nonlinear harmonics). The ratio between the complex Fourier terms of response and the force at the excitation frequency generates the frequency response. With the inclusion of a PID controller, able to control the amplitude of the steady state of the response for every linear excitation frequency, the *FRFs* can be "*linearised*" at a given constant response amplitude, and linear modal analysis methods can process the transfer functions. The higher the amplitude levels, the more the nonlinearity can be characterised [19] and [20]. In the nineties, Li [21] investigated a different technique for analysing nonlinear *FRFs* in his PhD thesis. It did not require a control method for acquiring vibrations but was based on the open-loop control technique. The identification method was based on analysing a nonlinear *FRF* by taking two pairs of frequency points at an equal vibration amplitude on either side of the response peak. One could write two receptance *FRF* equations at the same vibration amplitude, one for the frequency at the left and one at the right of the maximum response peak. These two equations, Real and Imaginary relationships, could be used to calculate the modal parameters. By sweeping the pair of frequency points from low up to high vibration amplitudes, the nonlinear *FRF* could be easily characterised. Carrella and Ewins [22] investigated this technique using an aerospace structure and evaluated its weaknesses. The method fails when one *FRF* branch is absent due to the system's unstable vibration response. Hence, the interpolation method used to identify the frequency points at the same displacement amplitude cannot be applied, so the equations cannot be solved correctly. Furthermore, the analysis is based on the single degree of freedom theory, which does not consider the contribution of neighbour modes. Although simple and practical, this experimental technique presents many limitations.

In recent years, Zhang and Zang [10-12] yielded several research papers presenting a method for identifying nonlinear modal parameters by measuring and analysing *FRFs*. Every *FRF* is measured by step-sine tests under steady state vibrations and labelled at drive voltage (V) feeding the shaker. The very innovative idea is to generate a three-dimensional response surface (such as acceleration) made of frequencies, voltages and accelerations (Hz, V, m/s^2) and a force surface made of frequencies, voltages and forces (Hz, V, N). The linearization process is achieved by extracting a constant acceleration curve from the acceleration surface and using it to extract the force curve. This operation is achieved using the common voltage axis to identify accelerations and forces. Once the operation is completed, the *FRF* linearised at the constant acceleration is derived. Finally, the linear modal analysis can extract the modal parameters. The more *FRFs* extracted from the surface, the better the nonlinearity characterisation is. The method is very robust for smooth and non-smooth types of nonlinearities. These techniques can calculate the amplitude-varying modal parameters from linear *FRFs*. The following subsection will propose a new technique derived from the line-fit method using the Dobson formulation. Before doing that, some basics of modal analysis using the inverse *FRF* methods are provided.

3.2 Inverse methods for modal analysis

The inverse *FRF* methods are commonly called single DoF modal analysis [1], because an *FRF* is analysed using the SDoF theory. The convenience of the analysis is that the inverse of an *FRF* can be separated into the Real and Imaginary parts and plotted as a function of the excitation frequency. Around the resonance, these two functions are straight lines, as becomes evident by inspecting the equation (22), where ω_r is the natural frequency, η_r is the damping loss factor of the r mode shape.

$$\alpha(\omega) = \frac{{}_rA}{\omega_r^2 - \omega^2 + i\zeta_r\omega\omega_r} = \frac{{}_rA}{\omega_r^2 - \omega^2 + i\eta_r\omega_r^2} \tag{22}$$

The modal constant ${}_rA$ in equation (22) can be either a Real or complex number. When the constant is a Real number, equation (22) can be inverted and separated into its real and imaginary parts, which can be plotted as a function of the squared excitation frequency, ω^2. The Real part of the equation (23) calculates the natural frequency. The Imaginary part of the same equation calculates either the loss factor or the damping ratio.

$$\alpha(\omega)^{-1} = RE + IM = \frac{\omega_r^2 - \omega^2}{{}_rA} + i\frac{\eta_r\omega_r^2}{{}_rA} = \frac{\omega_r^2 - \omega^2}{{}_rA} + i\frac{\zeta_r\omega\omega_r}{{}_rA} \tag{23}$$

When the constant ${}_rA = (A_r + iB_r)$ is a complex number, the inverse can be calculated by multiplying the numerator and denominator by its complex and conjugate, thus leading to (24). From this point, the manuscript will refer to a hysteretic damping model coherent with the Dobson formulation discussed hereafter.

$$\alpha(\omega)^{-1} = \frac{\omega_r^2 - \omega^2 + i\eta_r\omega_r^2}{{}_rA} = \frac{(A_r + B_r\eta_r)\omega_r^2 - A_r\omega^2}{A_r^2 + B_r^2} + i\frac{(A_r\eta_r + B_r)\omega_r^2 - B_r\omega^2}{A_r^2 + B_r^2} \tag{24}$$

The Real and Imaginary parts of the equation (24) are linear relationships as a function of ω^2, see equation (25). These two equations (25a&b) can be solved by calculating the coefficients and intercepts of the straight lines, which are used for evaluating the four modal properties $(\omega_r^2 \quad \eta_r \quad A_r \quad B_r)$.

$$RE(\alpha(\omega)^{-1}) = \frac{(A_r + B_r\eta_r)\omega_r^2 - A_r\omega^2}{A_r^2 + B_r^2} = m_R + n_R\omega^2 \quad \text{(a)}$$

$$IM(\alpha(\omega)^{-1}) = \frac{(A_r\eta_r + B_r)\omega_r^2 - B_r\omega^2}{A_r^2 + B_r^2} = m_I + n_I\omega^2 \quad \text{(b)} \tag{25}$$

Although very simple and intuitive, this method is limited by the upper and lower residuals, which are not eliminated. The technique works for well-spaced resonances but fails as soon as resonances become closer in frequency. As opposed to the simple line fit, Dobson [13] developed a method based on better mathematical formulation, which could eliminate the effect of the residuals from the analysis. Even though the Dobson method is applied to SISO tests, Maia extended the same method to Single-Input Multiple-Output (SIMO) tests [23]. Recalling the drive-point *FRF* in equation (26), the linear frequency response is the total sum of the contribution of *N* modes (r), or equally, the sum of a single mode (r) with a constant residual.

$$\alpha_{ii}(\omega) = \sum_{r=1}^{N} \frac{{}_rA_{ii}}{\omega_r^2 - \omega^2 + i\eta_r\omega_r^2} = \frac{{}_rA_{ii}}{\omega_r^2 - \omega^2 + i\eta_r\omega_r^2} + residual \tag{26}$$

The Dobson method introduces a new variable, a pseudo excitation frequency, Ω, which is used to build a pseudo response frequency, $\alpha(\Omega)$, near the resonance. The effect of residuals on the response of the mode (r) is eliminated by subtracting the two transfer functions, as presented in equation (27).

$$\alpha_{ii}(\omega) - \alpha_{ii}(\Omega) = \frac{A_r + iB_r}{\omega_r^2 - \omega^2 + i\eta_r\omega_r^2} - \frac{A_r + iB_r}{\omega_r^2 - \Omega^2 + i\eta_r\omega_r^2} =$$
$$(A_r + iB_r)\left[\frac{\omega^2 - \Omega^2}{(\omega_r^2 - \omega^2)(\omega_r^2 - \Omega^2) - \eta_r^4\omega_r^4 + i\eta_r\omega_r^2(2\omega_r^2 - \omega^2 - \Omega^2)}\right] \tag{27}$$

By multiplying the numerator of equation (27) by the complex and conjugate of the modal constant and by taking the inverse, one can define a function delta Δ, as expressed in equation (28).

$$\Delta = \frac{\omega^2 - \Omega^2}{\alpha_{ii}(\omega) - \alpha_{ii}(\Omega)} = \frac{A_r - iB_r}{A_r^2 + B_r^2}(\omega_r^2 - \omega^2)(\omega_r^2 - \Omega^2) - \eta_r^4\omega_r^4 + i\eta_r\omega_r^2(2\omega_r^2 - \omega^2 - \Omega^2) \tag{28}$$

The "fixing" frequency, Ω, will sweep the entire excitation frequency vector ω , thus generating an array $[\Delta]_{n\times n}$where the zeros obtained for $\Omega = \omega$ will need to be eliminated. The next step is to separate the real and imaginary deltas and plot them as a function of the frequency squared, ω^2, in equation (28).

$$RE(\Delta) = m_R\omega^2 + c_R$$
$$IM(\Delta) = m_I\omega^2 + c_I \tag{29}$$

The angular coefficients are expressed in equation (30).

$$m_R = -\frac{1}{A_r^2 + B_r^2}[A_r(\omega_r^2 - \Omega^2) + B_r\eta_r\omega_r^2]$$
$$m_I = -\frac{1}{A_r^2 + B_r^2}[B_r(\omega_r^2 - \Omega^2) - A_r\eta_r\omega_r^2] \tag{30}$$

The angular coefficients from the plots (RE(Δ), ω^2) and (IM(Δ), ω^2) are selected and used for generating two new straight lines, as expressed in equation (31). **Fig. 14** shows the implementation of the method.

$$m_R = n_R\Omega^2 + d_R$$
$$m_I = n_I\Omega^2 + d_I \tag{31}$$

One can solve the modal parameters using the relationships expressed in equation (32) by evaluating the two angular coefficients and intercepts of the two straight lines.

$$n_R = -\frac{(A_r + B_r\eta_r)\omega_r^2}{A_r^2 + B_r^2}$$
$$d_R = \frac{A_r}{A_r^2 + B_r^2} \tag{32}$$

$$n_I = -\frac{(A_r\eta_r - B_r)\omega_r^2}{A_r^2 + B_r^2}$$

$$d_I = -\frac{B_r}{A_r^2 + B_r^2}$$

The four constants evaluated by equation (32) can be used for extracting the four modal parameters $(\omega_r^2 \quad \eta_r \quad A_r \quad B_r)^{-1}$. The Dobson method proved robust because the procedure performs the line fitting twice before the modal parameters are extracted.

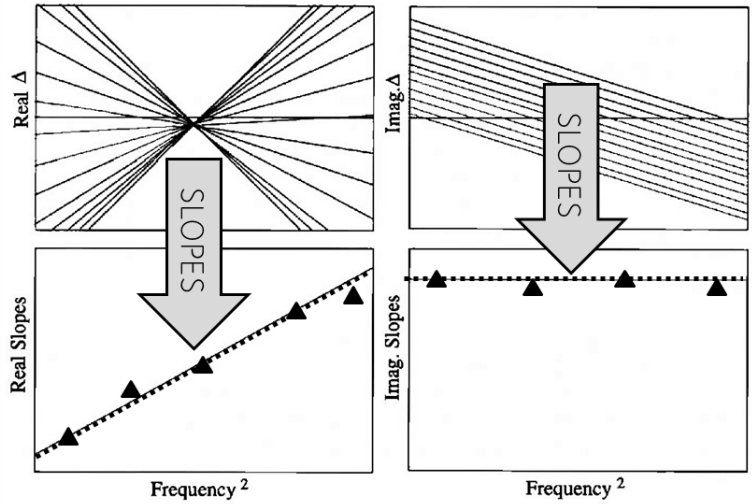

Fig. 14: Implementation of the Dobson method for a linear *FRF*. The slopes from the Real(Δ) and Imag(Δ) are selected and fitted again by straight lines

3.3 Modified-Dobson method applied to nonlinear *FRFs*

The previous subsection presented the Dobson method applied to a linear *FRF*. The author postulates that the same mathematical formulation can characterise nonlinear *FRF* and calculate the nonlinear modal parameters. First of all, a nonlinear *FRF* is plotted using the Nyquist circle. One shall think of a nonlinear *FRF* that starts from an underlying linear response, becoming increasingly nonlinear as one sweeps the Nyquist circle and then more and more linear as one approaches its origin again. The Nyquist points do not indeed form a circle, but it is possible to select three frequency points forming a Nyquist circle of an equivalent linear system. Assume that one takes two frequency points from the lowest amplitude of the *FRF* at which the vibration response can be considered linear.

Moreover, these two points can be taken on either side of the max response peak. Now, one shall assume that a third point is taken at any desired amplitude of the receptance, thus forming a triplet of frequency points. This triplet can form a Nyquist circle, identifying an equivalent linear system for the selected receptance amplitude. By sweeping the third receptance point from the first to the second reference point of the *FRF*, one can observe how the modal parameters change from linear to nonlinear vibrations. It is like performing a continuation analysis using the sweeper as an observer.

The data analysis is therefore carried out by selecting triplets of frequency responses at every iteration. These triplets are chosen as indicated in the previous paragraph. The two references are called the "*fixers*", and these two will never change during the Dobson analysis. The third frequency point, forming the triplet, is called the "*sweeper*" because it will change for every triplet. Therefore, a selected response peak of an *FRF* made of 32 frequency points will be analysed 30 times, such that three frequency points are taken for each analysis, as expressed in equation (33). The *sweeper* will sweep the frequency points between the two references.

$$\left(\alpha\left(\omega_1^{fxr}\right) \quad \alpha\left(\omega_i^{swp}\right) \quad \alpha\left(\omega_N^{fxr}\right)\right)^{-1} \qquad (33)$$
$$i = 2, \ldots, N-1$$

Therefore, the procedure is repeated from equation (26) up to (32) as often as needed for the *sweeper* to observe all the frequency points around the response peak. **Fig. 15** shows a diagram of the modified-Dobson implementation for the analysis of a nonlinear *FRF*, and it becomes more apparent when **Fig. 16** is also observed.

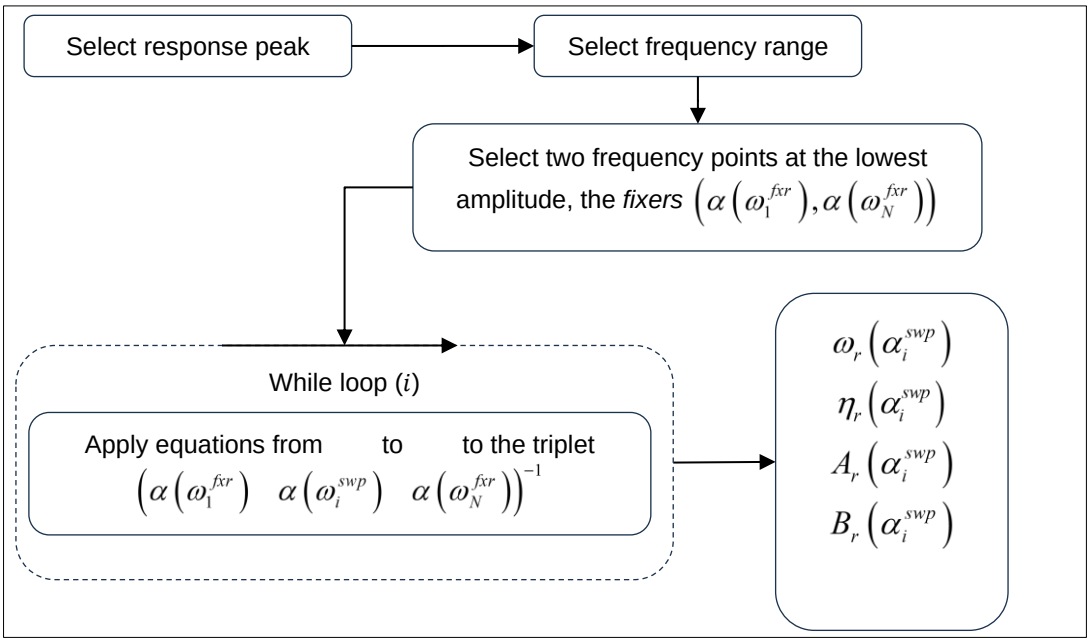

Fig. 15: Diagram of the modified-Dobson method

Fig. 16(a) shows the Nyquist circle, while **Fig. 16(b)** shows the moduli of the *FRF*s. The two frequency points in green are the *fixers*, and these are at low amplitudes where the vibration response is still linear, as visible in **Fig. 16(b)**. The third frequency point is the *sweeper*, in red, which can be taken anywhere between the two references, and the modal parameters will be a function of the modulus of the receptance, $\left|\alpha\left(\omega_i^{swp}\right)\right| = \alpha_i^{swp}$. This triplet can be used to generate the Nyquist circle of an equivalent linear system at the amplitude of the *sweeper*. The Dobson method is now applied to the triplet to extract the modal parameters at that given amplitude, as the diagram in **Fig. 15** describes.

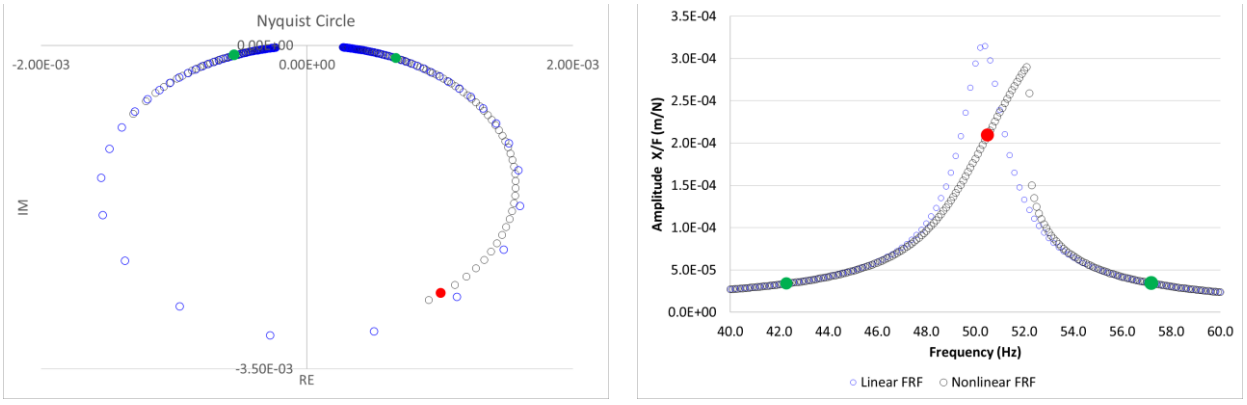

a) Nyquist plots b) Modulus of linear and nonlinear *FRF*

Fig. 16: Linear and nonlinear response functions, with fixers (green) and sweeper (red).

Fig. 17 shows one step of the straight-line fitting, as expressed in equation (29) and where the coefficients are expressed in equation (30). The natural frequency can be evaluated as a function of the amplitude of the *sweeper* by repeating the process as many times as required. **Fig. 17(a)** shows the Real part of the delta, while **Fig. 17(b)** shows the Imaginary part.

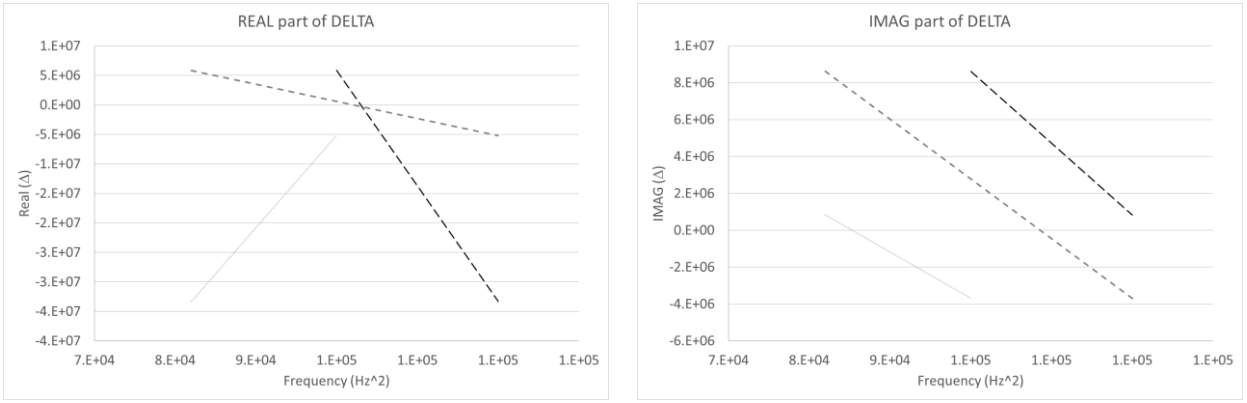

a) Real (Δ) of the first step analysis b) Imaginary (Δ) of the first step analysis

Fig. 17: The Real and Imaginary Δ of the first step analysis of one triplet

The red dot in **Fig. 18** indicates the natural frequency of an equivalent linear system at the amplitude of the *sweeper*. **Fig. 18** also shows the natural frequency curve where some points are circled in blue, indicating the natural frequency curve calculated when the *sweeper* goes beyond the response jump, from about 52 Hz up to 53 Hz. The modified-Dobson method is a simple and effective technique that overcomes two main shortfalls identified in the Lin's and the Zhang-Zang methods. The first one is limited when one of the two branches of the *FRF* is missed, as in the example presented in **Fig. 18**, because the algorithm needs two frequency points on either side of the max response peak of the *FRF*. The second method requires the measurement of a few nonlinear *FRFs* to extract linearised ones, which can be used to evaluate the modal parameters. The modified-Dobson method can extract the nonlinear modal parameters from a single *FRF*. The applicability of the modified-Dobson method is valid for well-separated resonances because equation (27) eliminates the residuals from neighbouring modes. Still, it fails when modes become closer and closer for two main reasons. For the first reason, the two references are taken at an amplitude with linear vibration. However, the closer the modes are, the higher the chances of including nonlinear residuals in frequency points taken as references. In the second one, the *sweeper* sweeps the frequency points from one fixer to the other, thus including different residuals at every iteration. The standard Dobson method equation (25) is calculated for as many frequency points as available in the analysis run, thus eliminating the residuals. In the present modified formulation, equation (27) is carried out for one triplet, which changes every time. The issue can be mitigated by including a technique called "interference criteria in modal identification" proposed by Maia [18].

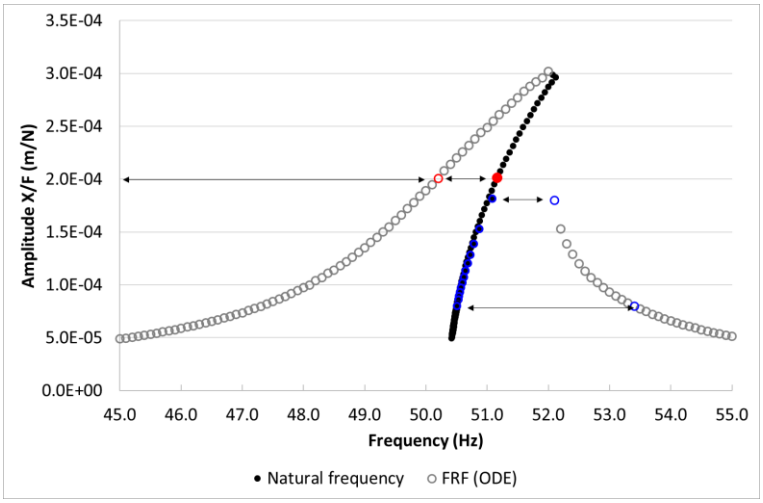

Fig. 18: Nonlinear *FRF* with natural frequency in black. The red dot indicates the linearised natural frequency at the amplitude of the *sweeper*.

Finally, having evaluated the modal parameters as a function of the amplitude of the *sweeper*, one shall convert those into polynomial functions. **Table 3** reports the steps to generate the polynomial functions.

Table 3: Summary table for the modal properties

Function of receptance	Function of displacement	Polynomial functions	Equations
$\omega_r\left(\alpha_i^{swp}\right)$	$\omega_r\left(X_i^{swp}\right)$	$\omega_r(X) = \omega_n X^n + \ldots + \omega_1 X + \omega_0$	(34)
$\eta_r\left(\alpha_i^{swp}\right)$	$\eta_r\left(X_i^{swp}\right)$	$\eta_r(X) = \eta_n X^n + \ldots + \eta_1 X + \eta_0$	(35)
$A_r\left(\alpha_i^{swp}\right)$	$A_r\left(X_i^{swp}\right)$	$A_r(X) = A_n X^n + \ldots + A_1 X + A_0$	(36)
$B_r\left(\alpha_i^{swp}\right)$	$B_r\left(X_i^{swp}\right)$	$B_r(X) = B_n X^n + \ldots + B_1 X + B_0$	(37)

$$\alpha(\omega, X) = \frac{{}_rA(X)}{\omega_r^2(X) - \omega^2 + i\eta_r(X)\omega_r^2(X)} \tag{38}$$

Equation (38) can be used to generate the experimental *nonlinear response frequency surface*.
It is worth mentioning that equation (38) is written as a function of displacement. However, it could be the same if the velocity or acceleration were measured, so one will deal with Mobility or Accelerance *FRFs*. The *nonlinear frequency response* surface will be coherent with the units used for the measurements, and conversions are always possible because the ratio is calculated with the fundamental excitation frequency. Equation (39) can be solved numerically,

$$|\tilde{\alpha}(\omega, X)| \left| \left(\frac{{}_rA(X)}{\omega_r^2(X) - \omega_{NL}^2 + i\eta_r(X)\omega_r^2(X)} \right)^{-1} \right| = 1 \tag{39}$$

as indicated in section 2.4, to find the nonlinear frequencies, ω_{NL}, of the nonlinear *FRF*.
The following section will demonstrate that the nonlinear *FRF* evaluated from the synthesised surface can be compared to the experimental one. The $|\tilde{\alpha}(\omega, X)|$ comes from the force surface used in section 2 to intercept the *nonlinear frequency response surface*.

4 Experimental validation

This section will describe the experimental validation of the modified-Dobson method and the application of the new method for extracting nonlinear *FRFs*. The validation is developed in four stages. The first experimental validation (setup-1) will verify that the proposed modified-Dobson method produces the same results as the Zhang-Zang method. The second and third experimental validations will verify that the new analysis method can calculate nonlinear *FRFs* once the nonlinear modal parameters are identified. These parameters are used to regenerate *FRFs* by the equation (38) to build the *NFRS*, from which the nonlinear *FRFs* are calculated. The final case is a blind analysis for which the author does not know the test article, measurement setup, and acquisition.

As mentioned earlier, equation (38) is a receptance model that converts to Mobility or Accelerance depending on the test data. Three test setups, built over the past ten years for different research reasons and applications, are used for this validation exercise.

4.1 Validation of the modified-Dobson method using setup-1

The experiment for validating the modified-Dobson method is made of a simple aluminium semicircle structure with two extremes connected by two strips of metals. The test structure is mounted by a load cell to the shaker head, while an accelerometer is connected to the side of the semicircle. **Fig. 19** shows the test structure and the setup with the shaker and sensors. The mode of vibration selected for this experiment is at approximately 326 Hz, which brings the two extreme points of the arch close and apart, thus forcing the thin metal strips into nonlinear vibrations.

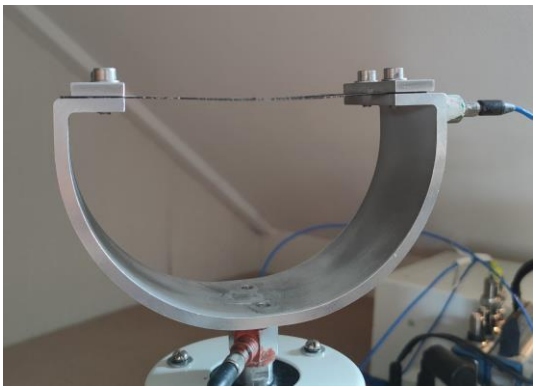

Fig. 19: Test structure for validation of the modified-Dobson method.

A custom-made acquisition panel was developed to measure the acceleration and force signals and calculate the transfer functions. The control panel stepped over the frequency range of interest using a drive signal for the shaker, shaped with a cosine tapered window. Therefore, every sinewave had a smooth ramp-up, steady state, and a smooth ramp-down signal. It avoided harsh transients from one frequency to the next one. An example of a response signal is available in Appendix A2, **Fig. A34**, which shows an example of the sinewaves measured by the accelerometer and force sensors, and where in red, the portion of the steady state signal is analysed. The test was conducted at ten drive voltages from 0.1V up to 1V, with a 0.1V increment.

The Zhang-Zang method was applied to the acceleration and force surfaces. The acceleration surface was cut by a plane at constant acceleration, and the voltage axis found the corresponding forces shared by the two surfaces. The standard Dobson method calculated and processed a set of linearised *FRFs* to extract the modal parameters. The modified-Dobson method processed the nonlinear *FRFs* generated using the steady state part of the acquired signals to extract amplitude-dependent modal parameters, as shown in **Fig. 20**. **Fig. 21** and **Fig. 22** show the natural frequency and damping curves for the stepwise and modified-Dobson analyses. The Zhang-Zang method confirms the results of the modified-Dobson method.

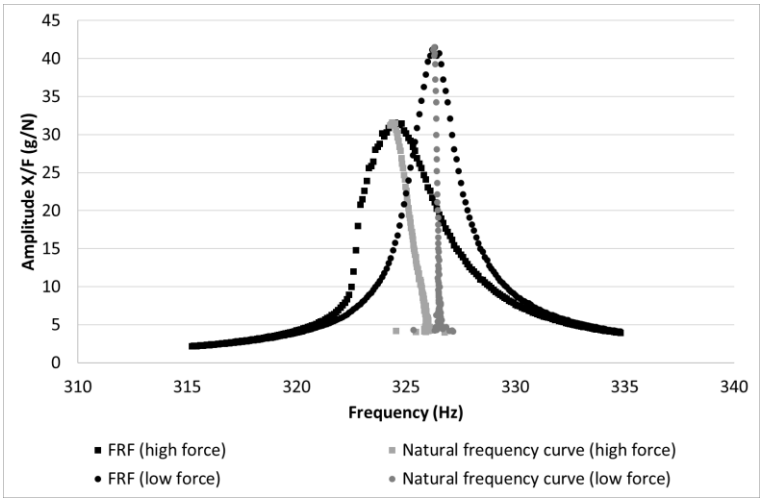

Fig. 20: Two nonlinear *FRFs* processed by the modified-Dobson method

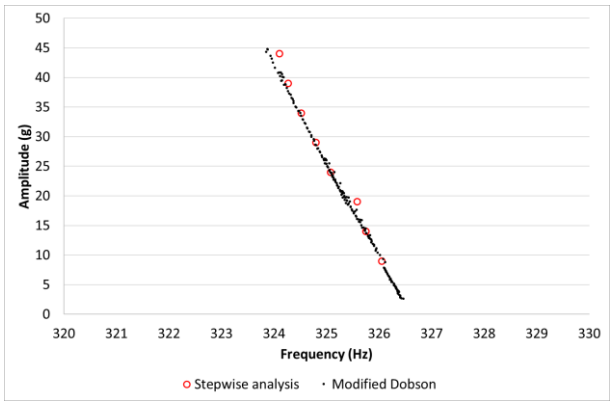

Fig. 21: Natural frequency curves compare modified-Dobson and stepwise analysis methods (note these are expressed in acceleration (g))

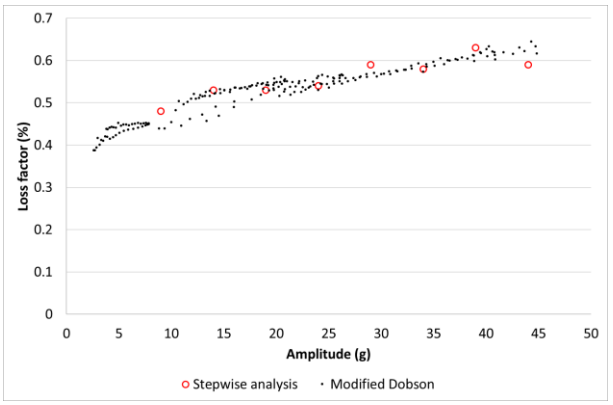

Fig. 22: Damping curves compare modified-Dobson and stepwise analysis methods

4.2 Validation of the new method for setup-2: a dumbbell setup

This first stage of the validation of the new method is based on an experiment carried out on a dumbbell setup with a shaker, as shown in **Fig. 23**. Most details are reported in [25]. This section will resume the central aspect of that publication. The test structure was designed to have two steel masses weighing approximately 4 kg. The lap joint comprises two square aluminium sections, each connected to the mass with a single 10/32 UNF bolt and coupled to each other with two M5 bolts. Two torque levels of 6 Nm and 10 Nm were applied to the bolts to track the behaviour differences. The structure was instrumented with four single-axis accelerometers placed at the ends of the cylinders, and a force gauge was installed in the axial direction. The dumbbell was then supported by two belts and suspended in *free-free* conditions by elastic cords.

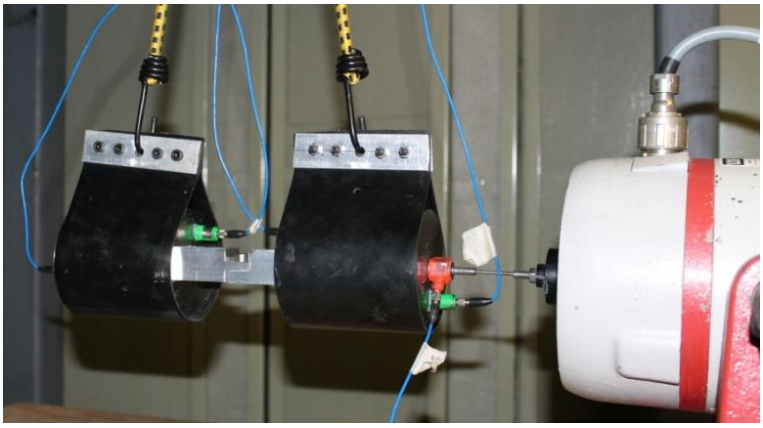

Fig. 23: Dumbbell test setup

The test regards the stepped sine excitation, which was carried out at pure tone excitation in a frequency range between 1200 [Hz] and 1360 [Hz] with a frequency resolution of 0.2 [Hz]. The test was carried out by controlling the excitation force, which was kept constant over the frequency range. These campaigns used several excitation forces, measured for a tightening torque of 6 Nm and 10 Nm, respectively. The measured *FRFs* showed an evident distortion of the response curves as the excitation force is increased, demonstrating the amplitude dependency of this nonlinear phenomenon under study. **Fig. 24** shows an example of *FRFs* measured at various excitation forces for a tightening torque 10 Nm. The *FRF* measured at 25 N is processed by the modified-Dobson method. The amplitude-dependent modal parameters were then used to generate the surface and calculate nonlinear *FRFs*. **Fig. 25** shows the black nonlinear *FRF* measured at 25 N, with the natural frequency curve in red. Polynomials fitted the four nonlinear modal parameters as a function of the modulus of the Accelerance of the sweeeper, $|A(\omega)| = \bar{A}$. Table 4 reports the polynomial functions used for generating the surface, recalling that those polynomials were converted to acceleration functions. The 3D surface plot is made by Accelerance (g/N), Frequency (Hz), Acceleration (g).

Table 4 Amplitude-dependent modal parameters in the form of polynomial functions

Modal parameters	Polynomial functions	Equations
Natural Frequency (Hz)	$\omega_r(\bar{A}) = 3.067 * \bar{A}^2 - 24.52 * \bar{A} + 1265.1$	(40)
Damping loss factor (-)	$\eta_r(\bar{A}) = 0.0006 * \bar{A} + 0.0082$	(41)
Modal constant - Real	$\mathrm{RE}\left({}_rA(\bar{A})\right) = -33975 * \bar{A}^2 - 136804 * \bar{A} + 891077$	(42)
Modal constant - Imaginary	$\mathrm{IM}\left({}_rA(\bar{A})\right) = 42430 * \bar{A} - 26831$	(43)

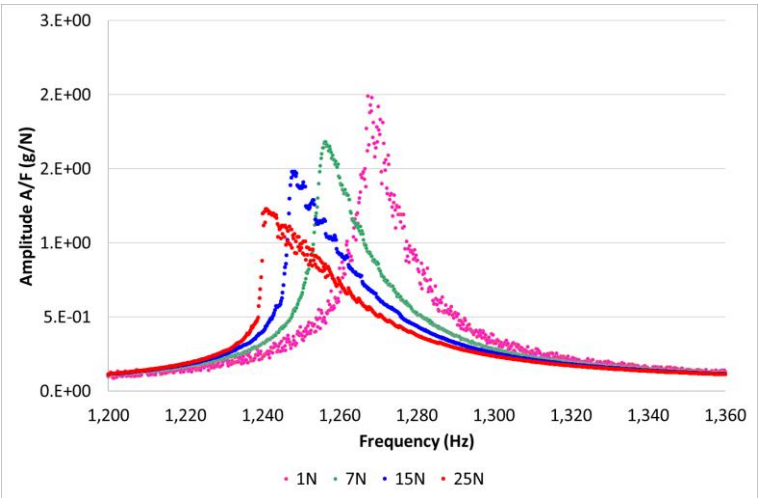

Fig. 24: Nonlinear *FRFs* at various force levels for 10Nm torque

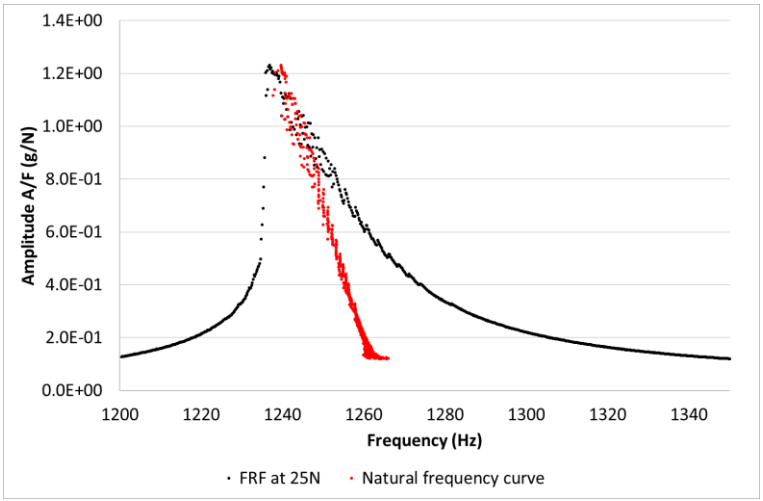

Fig. 25: Nonlinear *FRF* at 25 N in black with the natural frequency curve in red

The surface is graphically similar to the one shown in **Fig. 4** and is not reproduced here. The goal is to compare the experimental *FRF* at 25 N force with the regenerated one extracted from the *NFR* surface. Furthermore, it is expected that by changing the force magnitude (and so the inclination of the force plane), one can extract the regenerated *FRFs* of 15 N and 7 N force. **Fig. 26** shows the targeted *FRF* at 25 N measured and regenerated *FRFs* in red and black, respectively. The overlap is rather remarkable. Moreover, the figure also shows the overlay between the *FRFs* at 15 N (blue) and 7 N (green) and the regenerated nonlinear ones. Even for these two cases, the regenerated and measured ones overlay well.

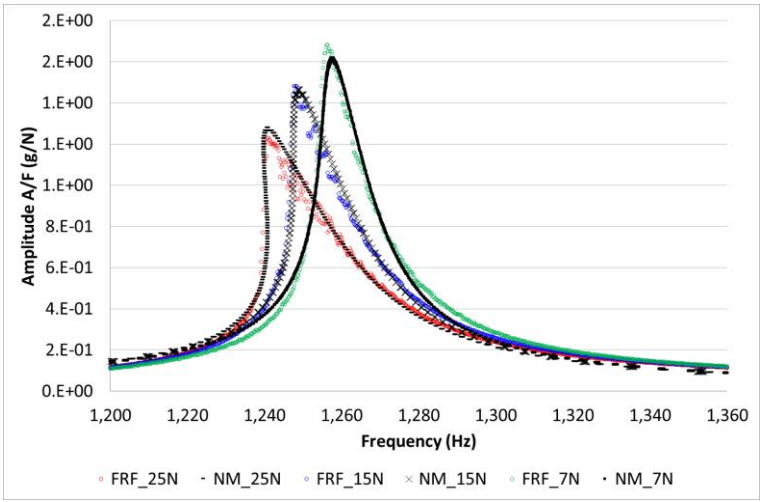

Fig. 26: Measured and regenerated nonlinear *FRFs.*

One final remark: the constant term of ω_r, equation (40), is not the natural frequency of the underlying linear system because the *FRF* is still mildly nonlinear. A much lower excitation force is required for extracting the linear natural frequency curve. The modified-Dobson observes the change of modal parameters from the lowest vibration points of the *FRF*, which are not always as low as desired for extracting the linear parameters.

4.3 Validation of the new method using setup-3: a composite blade

The third validation stage was carried out using *FRF* data measured from cantilever blades made of composite materials. The work was published in [26], and more details can be found in that manuscript. Here, a summary is given to the reader to contextualise the type of experiments executed on such test structures. The blades were designed using different layup configurations to enhance the nonlinear vibration response. Three different stacking sequences of composite materials were selected, and these were a unidirectional named (0-0), a cross-ply named (0-90) and a cross-ply named (+45, -45). The first three modes were investigated for each configuration. The measurements of the *FRFs* were carried out using a contactless excitation system called the Pulsed Air Jet system, which was developed by the author of this paper with the support of Rolls-Royce plc. [27] .

The excitation force was exerted onto the blade by jets of compressed air sampled by a spinning perforated disc. The rotational speed of the disc could be adjusted, and the jets' rate could be yielded to excite the resonances of the blade. The blade was mounted inside a mass block of about 40kg, where another smaller mass block was pressed utilising two large bolts, the root of the blade, as shown in **Fig. 27**. The nozzle of the Pulsed Air Jet was directed to the corner of the blade. This exciter is contactless, meaning the excitation force exerted by the compressed air jet cannot be measured. An attempt was made to calibrate the measured pressure at the nozzle with a load cell, but the results were not accurate. Therefore, the *FRFs* presented in this paper were scaled by an arbitrary constant unit force. A single-point laser vibrometer was used to measure the response at the blade's top-left (or top-right corner), as shown by the reflective tapes in **Fig. 27**. The *FRFs* were measured under steady state response, which meant changing the rotational speed step-by-step, with an elapsed time to settle the transient response. The acquisitions of the steady state signals were triggered by the one-pulse per revolution of an encoder mounted on the shaft of the rotor used to measure rotational speed. Such an acquisition arrangement allowed for measuring the modulus and phase of each spectral frequency point. The excitation level was changed manually by opening the compressed airflow's inlet valve to the exciter system's plenum chamber. Hence, this manual operation is another reason for scaling the force arbitrarily, set to unity for convenience.

Two examples of *FRFs* are presented here. The first one was measured from a blade made of cross-ply laminate, where the second bending mode of the blade was measured. The *FRF* was processed by the modified-Dobson method, and the nonlinear modal parameters were fitted by the polynomials function of the mobility *FRF* modulus $|V(\omega)| = \tilde{V}$, as shown in **Table 5**.

Fig. 27: Blade mounted onto a block with the nozzle of the exciter at the top-left corner

Fig. 28 shows the measured *FRF* (grey) with the frequency curve extracted by the modified-Dobson method (red) and the regenerated nonlinear *FRF* (black). The comparison is remarkable, so much so that the frequency curve could be seen continuing up to the peak displacement of the regenerated nonlinear *FRF*.

Table 5: Amplitude-dependent modal parameters (0-90) second bending resonance

Modal parameters	Polynomial functions	Equations
Natural Frequency (Hz)	$\omega_r(\bar{V}) = -2 * 10^8 * \bar{V}^3 + 748972 * \bar{V}^2 - 4057.6 * \bar{V} + 286.2$	(44)
Damping loss factor (-)	$\eta_r(\bar{V}) = -1378 * \bar{V}^2 + 5.3715 * \bar{V} + 0.0124$	(45)
Modal constant - Real	$\mathrm{RE}\left({}_rA(\bar{V})\right) = -13615 * \bar{V} + 17.522$	(46)
Modal constant - Imaginary	$\mathrm{IM}\left({}_rA(\bar{V})\right) = -4 * 10^8 * \bar{V}^3 - 1 * 10^7 * \bar{V}^2 + 31053 * \bar{V} + 175.6$	(47)

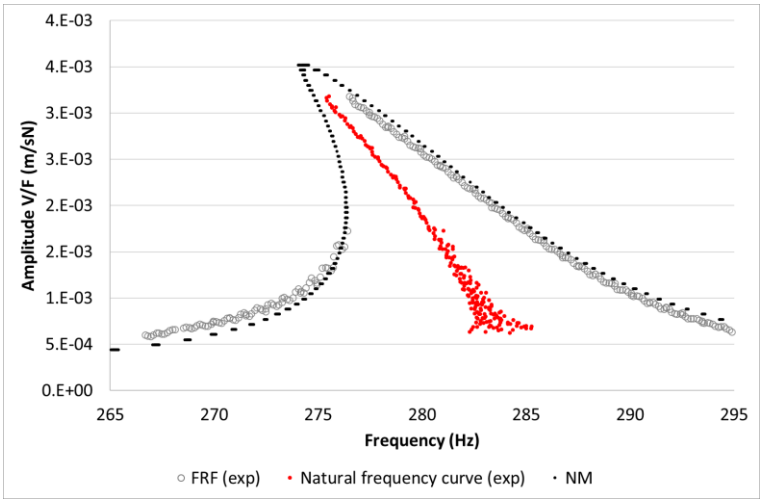

Fig. 28: Second bending mode of the composite blade (0-90).

Given the accurate regeneration of the nonlinear *FRF*, an attempt to extend the amplitude range of the previous regeneration was yielded. Therefore, the surface *FRF* and a new force surface were simulated to extract a new nonlinear *FRF*. The *nonlinear frequency response* surface is not reproduced because finding a suitable perspective to appreciate how the surface was shaped was impossible. **Fig. 29** shows a new *FRF* presenting the same curve seen in **Fig. 28** with an additional separate loop resembling an isola [28]. That feature might be a bias, or not, of the

polynomial function fitting the damping curve, which simulated a decrease of damping at higher vibration amplitudes. However, this matter was not investigated further.

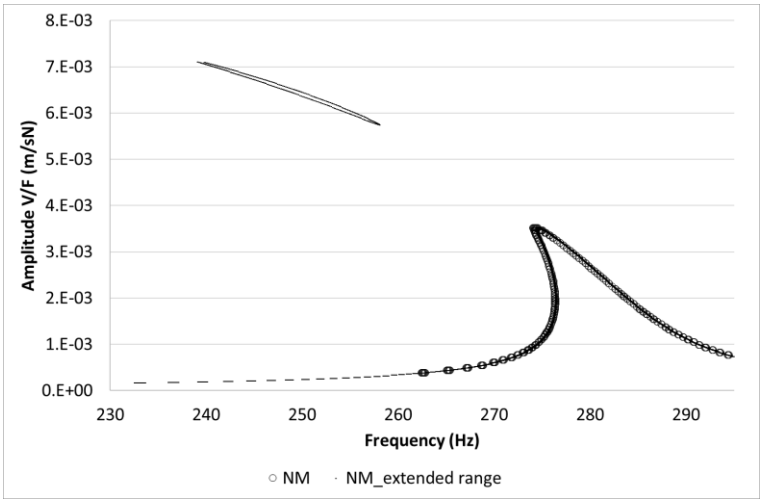

Fig. 29: Simulation with an extended amplitude range.

The last example describes the response measured from a composite blade made of a unidirectional laminate and vibrated at its first torsional mode. The experiment, the application of the modified-Dobson method, and the generation of the surface are the same as discussed earlier. **Table 6** shows the polynomial functions used for generating the surface.

Table 6: Amplitude-dependent modal parameters (0-0) first torsional resonance

Modal parameters	Polynomial functions	Equations
Natural Frequency (Hz)	$\omega_r(\bar{V}) = -2 * 10^9 * \bar{V}^3 + 5 * 10^6 * \bar{V}^2 - 1191.7 * \bar{V} + 306.24$	(48)
Damping loss factor (-)	$\eta_r(\bar{V}) = 0.016$	(49)
Modal constant – Real	$\mathrm{RE}\left({}_rA(\bar{V}) \right) = 6 * 10^9 * \bar{V}^3 - 1 * 10^7 * \bar{V}^2 + 889.38 * \bar{V} - 123.46$	(50)
Modal constant - Imaginary	$\mathrm{IM}\left({}_rA(\bar{V}) \right) = -8 * 10^9 * \alpha_{\bar{V}}^3 + 2 * 10^7 * \alpha_{\bar{V}}^2 - 5098.2 * \alpha + 35.035$	(51)

The damping was constant over the vibration amplitude analysed. Its value had to be slightly adjusted from 0.018 to 0.016 to match the peak amplitude of the regenerated *FRF* with the experimental one. **Fig. 30** shows the overlay of the experimental and regenerated *FRF*s, including the experimental natural frequency curve. The overlay shows a frequency offset caused by the natural frequency curve estimation. This divergence is caused by the selection of the frequency points swept by the *sweeper*, which were from a frequency at approx. 307 Hz up to 330 Hz. The whole frequency response curve was not used because the lower branch did not produce coherent modal parameters. Unfortunately, no alternative *FRF* was inspected for such typical *S*-shaped behaviour. Nonetheless, the overlay shows very similar shapes.

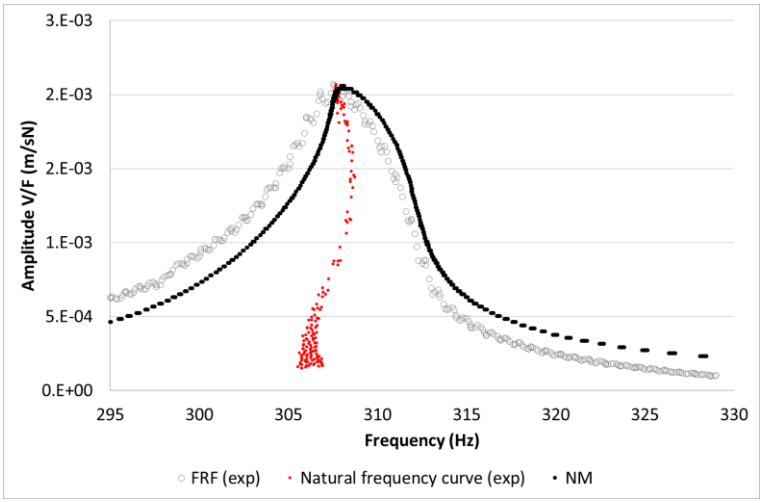

Fig. 30: Measured (grey) and regenerated (black) nonlinear *FRFs.*

4.4 Blind analysis cases

The final example is the analysis carried out on the test data of unknown components. The test data were received as transfer functions. There was no indication of the type of excitation signal used, nor was the vibration amplitude level reached to generate the nonlinear test data. The analysis followed the same procedure described in the previous examples. The modified-Dobson method was used for the sweep-up and sweep-down test data, and polynomial functions were evaluated for the nonlinear modal parameters. The test data were assumed Mobility transfer functions by inspecting the Nyquist circle. The polynomial functions of the modal properties are not reported in this section. **Fig. 31** shows the frequency response measured from high to low excitation frequency in red, while the blue curves show it measured the other way around. The regenerated *FRFs* were obtained from the nonlinear modal analyses of the red and blue curves, respectively. The regenerated curves show almost an identical profile; the one generated from the “measured – sweep up” roll off earlier than the other one. Both regenerated nonlinear responses do not sufficiently capture the region of the unstable response, which is the frequency band between the red and blue curves. The regenerated *FRFs* tend to fold but not sufficiently enough. This inaccuracy could be an issue with the modal analysis and regeneration or measurement bias. It is difficult to judge, given the blind analysis exercise.

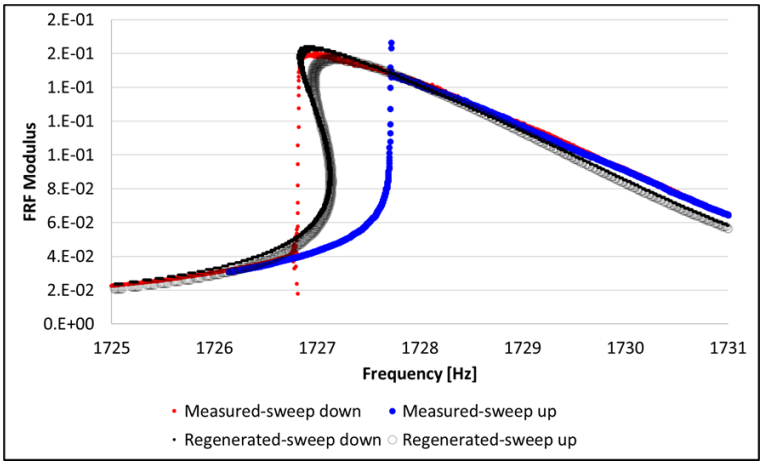

Fig. 31: Measured (blue and red) and regenerated (grey and black) nonlinear *FRFs.*

Fig. 32 shows another example, where both measured (red) and regenerated (black) are overlaid to verify the consistency of the modal parameters derived by the modified-Dobson method. Both examples demonstrate that test data, probably archived, can now be processed and verified.

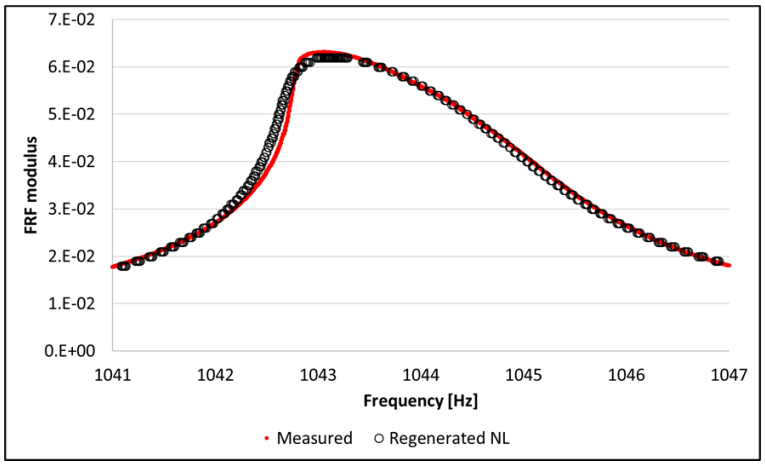

Fig. 32: Measured and regenerated frequency responses

5 Discussions

In the introduction, the manuscript postulated the following hypothesis: *A nonlinear frequency response surface, generated by a waterfall of linear FRFs, is the solution space of nonlinear FRFs, which can be evaluated by any force plane cutting across the response surface.* The first scientific challenge to address was to develop a new mathematical formulation to (i) analyse a *nonlinear frequency response surface* and (ii) calculate nonlinear frequency response functions. ONE and TWO-DoF response models were used to explain how the *NFRS* could be generated using linear frequency response functions, each starting with a different equivalent stiffness. Although a simple ground nonlinearity was used, the theoretical formulation allowed us to understand that any nonlinear *FRFs* could be evaluated from that surface. The nonlinear *FRF* is the result of a geometrical intersection between two surfaces. This calculation is simple and essential for the following challenge: when the *NFRS* is generated using nonlinear modal parameters extracted from the measurements. Even though the proposed analysis presents some similarities with the ones proposed by Özgüven [9], Schwartz [29] and Scheel [30], the main difference lies in using linear *FRFs* to generate a *nonlinear frequency response surface*.

The second scientific challenge was to develop a new modal analysis tool to calculate amplitude-dependent modal parameters reformulating Dobson line-fit method. The modified-Dobson formulation allowed the calculation of the nonlinear modal parameters. The reformulation of the line-fit method allowed the deconstruction of a nonlinear *FRF* in many linear ones by using a triplet of frequency points at the time. A significant benefit was given by the sweeper, which swept the response frequency even when one branch of the response was missing. The experimental analysis indicated that a well-isolated resonance could be identified, and nonlinear *FRFs* could be regenerated and compared to the experimental ones. The challenge is when the modes become closer, whereby the current formulation might fail to return reliable nonlinear modal parameters. It was already stated in section 3.3 that the close modes analysis was addressed for the linear modal analysis, and a similar approach can be extended to the nonlinear one. This new modal analysis method is proven for single-input, single-output (SISO) testing and could be extended to single-input, multi-output (SIMO) tests. The convenience of this method is analyse *FRFs* measured with an open loop control scheme, which can be considered the most straightforward testing approach. A blind analysis was eventually carried out to validate three steps. The first was to use the modified-Dobson method to calculate the nonlinear modal data. The second step was to use those parameters to generate the *NFRS.* The third and final step was to evaluate nonlinear *FRFs* to compare with the measured ones.

The proposed new analysis method fills a gap in the modal analysis practice when test data are generated but cannot be analysed in any other way. Equally, the proposed method is not exclusive because it was applied to test data generated by the force-controlled using the closed-loop technique in section 4.2.

6 Conclusions

The primary objective of this manuscript was to enable engineers to analyse, regenerate and compare nonlinear *FRFs*, following a similar process established for linear modal analysis. This goal was achieved for *FRFs* measured under steady-state vibrations, smooth nonlinearities and well-separated modes. These conditions are not always possible for mechanical systems. Nonetheless, it was essential to (i) establish a new analytical framework for processing nonlinear frequency responses, (ii) regenerate, and (iii) compare them. The manuscript presented a modified-Dobson method for extracting nonlinear modal parameters. The experimental validation proves the new analysis method is user-friendly, time-efficient and reliable, producing good agreement between measured and synthesised nonlinear *FRFs*.

Acknowledgements

I wish to acknowledge Prof. David Ewins, with whom I exchanged uncountable thoughts about modal analysis. I would also like to acknowledge Mr. Jip van Tiggelen for the support offered during the write-up of this manuscript.

References

[1] D. J. Ewins, 1984. Modal Testing: theory, practice and application. Research Studies Press (RSP).
[2] Maia, N.M.M. and Montalvão e Silva, J.M., 1997. Theoretical and experimental modal analysis.
[3] Avitabile, P., 2017. Modal testing: a practitioner's guide. John Wiley & Sons.
[4] Worden, K., 2019. Nonlinearity in structural dynamics: detection, identification and modelling. CRC Press.
[5] Noël, J.P. and Kerschen, G., 2017. Nonlinear system identification in structural dynamics: 10 more years of progress. Mechanical Systems and Signal Processing, 83, pp.2-35.
[6] Tanrikulu, O., Kuran, B., Özgüven, H.N. and Imregun, M., 1993. Forced harmonic response analysis of nonlinear structures using describing functions. AIAA journal, 31(7), pp.1313-1320.
[7] Kuran, B. and Özgüven, H.N., 1996. A modal superposition method for non-linear structures. Journal of Sound and vibration, 189(3), pp.315-339.
[8] Ferhatoglu, E., Cigeroglu, E. and Özgüven, H.N., 2020. A novel modal superposition method with response dependent nonlinear modes for periodic vibration analysis of large MDOF nonlinear systems. Mechanical Systems and Signal Processing, 135, p.106388.
[9] Karaağaçlı, T. and Özgüven, H.N., 2021. Experimental modal analysis of nonlinear systems by using response-controlled stepped-sine testing. Mechanical Systems and Signal Processing, 146, p.107023
[10] Zhang, G., Zang, C. and Friswell, M.I., 2019. Identification of weak nonlinearities in MDOF systems based on reconstructed constant response tests. Archive of Applied Mechanics, 89, pp.2053-2074.
[11] Zhang, G., Zang, C. and Friswell, M.I., 2020. Measurement of multivalued response curves of a strongly nonlinear system by exploiting exciter dynamics. Mechanical Systems and Signal Processing, 140, p.106474.
[12] Zhu, T., Zhang, G. and Zang, C., 2022. Frequency-domain nonlinear model updating based on analytical sensitivity and the Multi-Harmonic balance method. Mechanical Systems and Signal Processing, 163, p.108169.
[13] Dobson, B.J., 1987. A straight-line technique for extracting modal properties from frequency response data. Mechanical Systems and Signal Processing, 1(1), pp.29-40.
[14] Salter, J.P., 1969. Steady State Vibration. Havant. Hampshire: Mason Press.
[15] Kerschen, G., Worden, K., Vakakis, A.F. and Golinval, J.C., 2007. Nonlinear system identification in structural dynamics: current status and future directions. In 25th international modal analysis conference.
[16] Singh, A., Allen, M.S. and Kuether, R.J., 2023. Multi-mode quasi-static excitation for systems with nonlinear joints. Mechanical Systems and Signal Processing, 185, p.109601.
[17] Magi, F., Di Maio, D. and Sever, I., 2017. Validation of initial crack propagation under vibration fatigue by Finite Element analysis. International Journal of Fatigue, 104, pp.183-194.
[18] Di Maio, D., Voudouris, G. and Sever, I.A., 2022. Investigation of fatigue damage growth and self-heating behaviour of cross-ply laminates using simulation-driven dynamic test. International Journal of Fatigue, 155, p.106617.
[19] Göge, D., Sinapius, M., Füllekrug, U. and Link, M., 2005. Detection and description of non-linear phenomena in experimental modal analysis via linearity plots. International Journal of Non-Linear Mechanics, 40(1), pp.27-48.
[20] Di Maio, D., Schwingshakl C. and Sever I. Development of a test planning methodology for performing experimental model validation of bolted flanges, Journal of Nonlinear Dynamics, Vol.81, n.4, 2015, DOI 10.1007/s11071-015-2382-9. (2015)
[21] R. Lin, Identification of the dynamic characteristic of nonlinear structures, Ph.D. Thesis, Department of Mechanical Engineering, Imperial College, London, 1990.
[22] Carrella, A. and Ewins, D.J., 2011. Identifying and quantifying structural nonlinearities in engineering applications from measured frequency response functions. Mechanical Systems and Signal Processing, 25(3), pp.1011-1027.
[23] Maia, N.M., 1992. A Global Version of Dobson's Method. In Proceeding of the International Modal Analysis Conference (pp. 907-907). SEM Society for Experimental Mmechanics INC.
[24] Maia, N. M. M. “Interference Criteria In Modal Identification” M. SC. Thesis, Technical University of Lisbon, 1985 (in Portuguese).
[25] Carri, A.D., Di Maio, D., Lucchetti, A. and Sever, I.A., 2014. Experimental model validation of a non-linear structure with lap-joint using the physical space approach. In 26th International Conference on Noise and Vibration Engineering, ISMA 2014 (pp. 1185-1198). Katholieke Universiteit Leuven.
[26] R. Di Sante and D. Di Maio. “Measurement of non-linear vibration response in aerospace composite blades using pulsed airflow excitation” Measurement, Volume 160, (2020).
[27] Di Maio, D. and Magi, F., 2015. Development of testing methods for endurance trials of composites components. Journal of Composite Materials, 49(24), pp.2977-2991.

[28] Detroux, T., Noël, J.P., Virgin, L.N. and Kerschen, G., 2018. Experimental study of isolas in nonlinear systems featuring modal interactions. Plos one, 13(3), p.e0194452.
[29] Schwarz, S., Kohlmann, L., Hartung, A., Gross, J., Scheel, M. and Krack, M., 2020. Validation of a turbine blade component test with frictional contacts by phase-locked-loop and force-controlled measurements. Journal of Engineering for Gas Turbines and Power, 142(5), p.051006.
[30] Scheel, M., Peter, S., Leine, R.I. and Krack, M., 2018. A phase resonance approach for modal testing of structures with nonlinear dissipation. Journal of Sound and Vibration, 435, pp.56-73.

APPENDIX

This appendix provides supporting materials:
1- A diagram to implement the new analysis method
2- Example of time domain data used for section 4.1.

A1 Block diagram to operate the new analysis method

The block diagram presented in **Fig. A33** shows a stepwise approach of the proposed new analysis method. Note that the look-up table requires the parameters' curves to create much finer steps than an analysis can typically produce. Hence, many interpolation points can be created between the ones identified by the modified-Dobson method. Remembering that the look-up table is also limited to the maximum vibration amplitude analysed is also good, for this case, the range cannot extended as it is possible for polynomial functions.

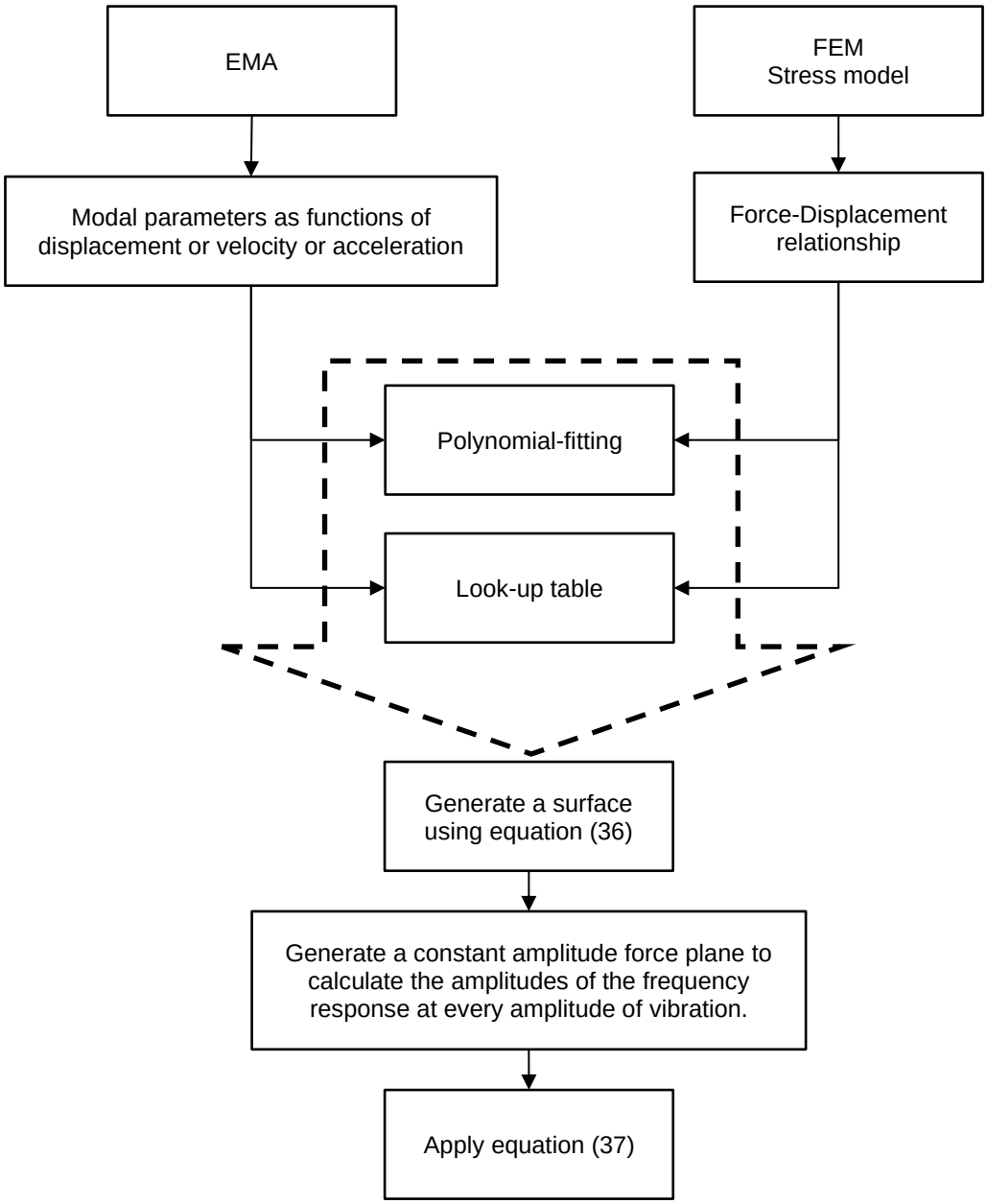

Fig. A33 Block diagram for the application of the new analysis method.

A2 Validation of the modified-Dobson method

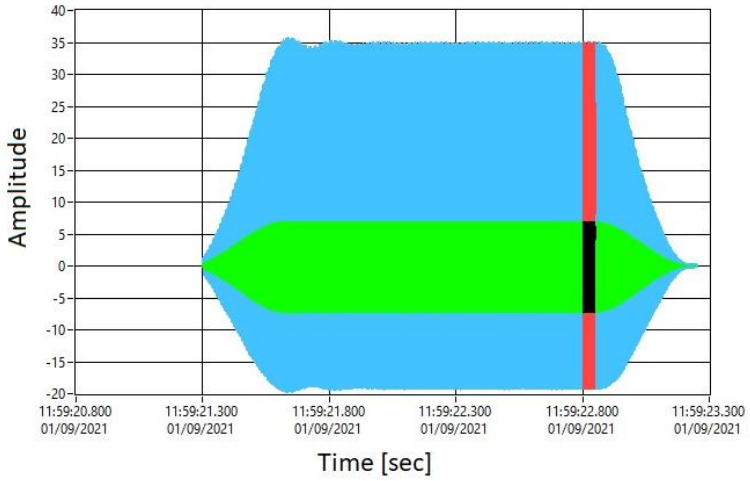

Fig. A34: An example of a signal measured by the accelerometer and force sensors. In red, the steady state part is analysed